Radial transport of dust in spiral galaxies

E. I. Vorobyov [a,b], Yu. A. Shchekinov [c]

[a] *Department of Physics and Astronomy, University of Western Ontario, London, Ontario, N6A 3K7, Canada*

[b] *Institute of Physics, Stachki 194, Rostov-on-Don, Russia*

[c] *Department of Physics, Rostov State University, Rostov on Don, Russia*

Abstract

Motivated by recent observations which detect dust at large galactocentric distances in the disks of spiral galaxies, we propose a mechanism of outward radial transport of dust by spiral stellar density waves. We consider spiral galaxies in which most of dust formation is localized inside the corotation radius. We show that in the disks of such spiral galaxies, the dust grains can travel over radial distances that exceed the corotation radius by roughly 25%. A fraction of the dust grains can be trapped on kidney-shaped stable orbits between the stellar spiral arms and thus can escape the destructive effect of supernova explosions. These grains form diffuse dusty spiral arms, which stretch 4-5 kpc from the sites of active star formation. About 10% of dust by mass injected inside corotation, can be transported over radial distances $3-4$ kpc during ≈ 1.0 Gyr. This is roughly an order of magnitude more efficient than can be provided by the turbulent motions.

Key words: galaxies: spiral, ISM: dust
PACS: 98.58.Ca, 98.52.NR

1 Introduction

Interstellar dust has been recently recognized to spread over large distances from their source, and thus can be considered as a tracer of dynamical processes responsible for the circulation of material in disk galaxies. Observations of edge-on galaxies reveal a great amount of dust far outside the galactic planes: in NGC 891 and NGC 4212 dusty clouds extend up to $z \sim 2$ kpc above

Email addresses: vorobyov@astro.uwo.ca (E. I. Vorobyov), yus@phys.rsu.ru (Yu. A. Shchekinov).

the plane, and contain in total as much as $\sim 10^8\ M_\odot$ (Howk and Savage, 1997, 1999; Rossa et al., 2004, Thompson et al., 2004). Several mechanisms can contribute to transport of dust in the vertical direction: convective motions or bore flows (Gómez and Cox, 2002) associated with spiral density waves, chimneys produced by multiple supernova explosions (Norman and Ikeuchi, 1989), and radiation pressure (Ferrara et al., 1991; Shustov and Vibe, 1995; Dettmar et al., 2005).

The situation is less clear when the radial distribution of dust is considered. Observations of spiral galaxies in the far infrared band show that dust can extend in the radial direction far beyond the stellar disks. Neininger et al. (1996) found that the radial distribution of 1.2 mm dust emission from NGC 4565 is two times wider than CO emission. ISO observations of several spiral galaxies at 200 μm (Trewhella et al., 2000; Bianchi et al., 2000) revealed the presence of relatively cold dust outside the stellar disks with a scale length $R_d \gtrsim 1.5\ R_*$ (R_d and R_* are the radial scales of dust and stars, respectively). A similar conclusion was made by Xilouris et al. (1999) for four spirals observed in the optical and near infrared bands. Bianchi et al. (2000) found that the best fit of the 200 μm emission for NGC 6946 gives $R_d \gtrsim 3\ R_*$. MHD turbulence can, in principle, spread dust outward in radial direction (Cho et al., 2003), however, the corresponding time for galactic scales seems to be too long. Indeed, the coefficient of turbulent diffusion $D \sim \langle Lv \rangle / 3$ is of the order of 10^{26} cm^2 s^{-1} for typical interstellar values $L \sim 100$ pc and $v \sim 10$ km s^{-1}. Therefore, dust particles can diffuse by turbulent motions over scales $\sqrt{\langle \Delta R^2 \rangle} > 3$ kpc in a characteristic time $t > 16$ Gyr. In these conditions, only regular hydrodynamic motions can explain the presence of dust outside stellar disks in spiral galaxies.

In this paper we explore the possibility that the radial transport of dust in spiral galaxies is driven by the hydrodynamic motions associated with spiral stellar density waves. In Sect. 2 a set of model hydrodynamic equations for dusty interstellar medium is described and the equilibrium parameters are fixed. In Sect. 3 the generation of spiral pattern in the stellar disk is formulated. Sect. 4 describes trajectories of single dust particles and Sect. 5 describes the dynamics of dust fluid as a whole including formation of dusty spiral arms. Sect. 6 summarizes our results.

2 Model description

2.1 Basic equations

Our model disk is a two-fluid system composed of dust and gas, which evolves in the external potential of the stellar disk and dark matter halo. We assume that the dust and gas are coupled by friction. The gas disk is isothermal at $T = 10^4$ K and the dust pressure is negligible. We use the thin disk approximation, i.e. all quantities are vertically integrated. The system is described by the basic hydrodynamic equations, where we denote the dust and gas by the subscripts d and g, respectively.

The continuity equation for the gas and dust is

$$\frac{\partial \Sigma_{\rm g,d}}{\partial t} + \boldsymbol{\nabla} \cdot (\Sigma_{\rm g,d}\, \boldsymbol{v}_{\rm g,d}) = 0, \tag{1}$$

where $\Sigma_{\rm g,d}$ are the gas and dust surface densities and $\boldsymbol{v}_{\rm d,g}$ are their velocities.

The equations of motion are

$$\frac{\partial \boldsymbol{v}_{\rm g}}{\partial t} + (\boldsymbol{v}_{\rm g} \cdot \boldsymbol{\nabla})\boldsymbol{v}_{\rm g} = -\boldsymbol{\nabla}\Phi_{\rm s1,s2,h} - \frac{\boldsymbol{\nabla} P_{\rm g}}{\Sigma_{\rm g}} + \frac{\Sigma_{\rm d}\boldsymbol{f}}{\Sigma_{\rm g}}, \tag{2}$$

$$\frac{\partial \boldsymbol{v}_{\rm d}}{\partial t} + (\boldsymbol{v}_{\rm d} \cdot \boldsymbol{\nabla})\boldsymbol{v}_{\rm d} = -\boldsymbol{\nabla}\Phi_{\rm s1,s2,h} - \boldsymbol{f}, \tag{3}$$

where, $\Phi_{\rm s1}, \Phi_{\rm s2}$, and $\Phi_{\rm h}$ are the contributions to the total gravitational potential by the axisymmetric stellar disk, non-axisymmetric spiral density perturbation, and dark matter halo, respectively. The friction force is defined as $\boldsymbol{f} = A(\boldsymbol{v}_{\rm d} - \boldsymbol{v}_{\rm g})$ (see Draine and Salpeter, 1977; Noh et al., 1991).

We take the friction coefficient A to be a simple function of the disk conditions. We assume that the thickness of the dust disk is comparable to that of the gas disk. Then the collisional timescale $\tau_{\rm c}$ of energy and momentum exchange between the gas and dust particles may be used as an estimate of A^{-1},

$$A \sim \tau_{\rm c}^{-1} = \frac{\sigma_{\rm c} n_{\rm g} v_{\rm th} m_{\rm g}}{m_{\rm d}}, \tag{4}$$

where $n_{\rm g}$ is the number density of gas particles, $m_{\rm g}$ and $m_{\rm d}$ are the masses of gas and dust particles, and $v_{\rm th} = \sqrt{3RT/\mu}$ is the gas velocity dispersion; $\tau_{\rm c}$ is estimated for the subsonic relative motion of neutral dust grains and gas. Since we use the thin disk approximation, the gas volume density in Eq. (4) is approximated assuming a local vertical hydrostatic equilibrium $m_{\rm g} n_{\rm g} = \Sigma_{\rm g}/z_0$,

where the gas disk thickness is defined as[1] $z_0 = 2c_s^2/(\pi G\Sigma_{\rm g})$, where $c_{\rm s}$ is the sound speed. The geometrical cross section is used as an estimate of the collisional cross section $\sigma_{\rm c} = \pi a^2$, where a is the average radius of a dust particle. In the present simulations, we assume $m_{\rm d} = 10^{-14}$ g and $a = 10^{-5}$ cm. It is well known that interstellar dust grains are charged, and Coulomb interactions with charged ambient ions and electrons increase the friction force (Draine and Salpeter, 1979; Weingartner and Draine, 2001). However, as we are mostly concerned with the diffuse HI phase of the ISM (warm neutral medium, WNM, in standard nomenclature), this increase does not crucially change the resulting friction coefficient. Indeed, the Coulomb friction can be written as $F_{\rm C} = \chi(Z)F^0_{\rm HI}$, where $F^0_{\rm HI}$ is the friction in an HI environment, $\chi(Z) = \langle a_Z/a\rangle^2 \ln\Lambda \sum\limits_i x_i(m_i/m_p)$, $a_Z = Ze^2/kT$, $\ln\Lambda$ is the Coulomb logarithm, x_i is the fractional ionization of i-th ions or electrons, m_i is the corresponding mass, averaging is over charge distribution of dust grains (Weingartner and Draine, 2001). For typical conditions in the WNM; $x \sim 0.1$, $n \sim 0.3$ cm^{-3}, and dust charge $\langle Z\rangle \simeq 60$ (Yan et al., 2004) we get $\chi \sim 1$. Therefore, we will restrict our consideration with the friction coefficient A as determined for the neutral dust.

2.2 Equilibrium gas disk

Initially, our model galaxy consists of a rotating gas disk balanced by the gravity of an *axially symmetric* stellar disk and spherically symmetric dark matter (DM) halo. The dust disk is introduced later when the non-axisymmetric part of the stellar gravitational potential is set. The rigid stellar disk is assumed to have a power-law radial density profile of the form

$$\Sigma_{\rm s}(r) = \frac{B^2}{2\pi G}\left[(r_{\rm s}^2 + r^2)^{-3/2}\right], \tag{5}$$

where $B^2 = 2\pi G r_{\rm s}^3 \Sigma_{\rm s0}$. The gravity force of such a density distribution is given by Toomre (1963)

$$\frac{\partial\Phi_{\rm s1}}{\partial r} = B^2\left[\frac{r}{r_{\rm s}}(r_{\rm s}^2 + r^2)^{-3/2}\right]. \tag{6}$$

In the following, we use the central stellar density $\Sigma_{\rm s0} = 1.2\times10^3\ M_\odot$ pc^{-2} and $r_{\rm s} = 3$ kpc, which gives us a total stellar mass of $M_{\rm st} = 7\times10^{10}\ M_\odot$.

[1] Since the dominant component of gravity in the vertical direction is the stellar disk, the total surface density ($\Sigma_{\rm tot} = \Sigma_{\rm g} + \Sigma_{\rm s}$) should appear in the expression for z_0. This may increase the friction coefficient A, especially in the inner regions. We discuss this issue in Sect. 5

The density distribution of the rigid DM halo is assumed to be that of a modified isothermal sphere (Binney and Tremaine, 1987)

$$\rho_{\rm h} = \frac{\rho_{\rm h0}}{(1 + r/r_{\rm h})^2}, \tag{7}$$

where the central density $\rho_{\rm h0}$ and the characteristic scale length $r_{\rm h}$ are given by Mac Low and Ferrara (1999) and Silich and Tenorio-Tagle (2001):

$$\rho_{\rm h0} = 6.3 \times 10^{10} \left(\frac{M_{\rm h}}{M_\odot}\right)^{-1/3} \; h^{-1/3} \; M_\odot \; {\rm kpc}^{-3} \tag{8}$$

$$r_{\rm h} = 0.89 \times 10^{-5} \left(\frac{M_{\rm h}}{M_\odot}\right)^{1/2} \; h^{1/2} \; {\rm kpc}. \tag{9}$$

Here, h is the Hubble constant in units of 100 km s^{-1} Mpc^{-1} and $M_{\rm h} = 10^{12}\ M_\odot$ is the total DM halo mass. We note that the DM halo mass within the computational domain $r < 20$ kpc is $M_{\rm h}(r < 20\ {\rm kpc}) = 5 \times 10^{10}\ M_\odot$. We adopt $h = 0.65$ throughout the paper. The gravitational force of spherically symmetric DM halo can be expressed as

$$\frac{\partial \Phi_{\rm h}}{\partial r} = 4\pi G \rho_{\rm h0} r_{\rm h} \left[r/r_{\rm h} - \arctan(r/r_{\rm h})\right] \left(\frac{r_{\rm h}}{r}\right)^2. \tag{10}$$

The gas disk has an exponentially declining density profile with the central surface density $\Sigma_{\rm g0} = 30\ M_\odot\ {\rm pc}^{-2}$, and radial scale length $r_{\rm g} = 9$ kpc. The total mass of the gas disk within the computational domain ($r = 20$ kpc) is $M_{\rm g} = 1.0 \times 10^{10}\ M_\odot$. The gas disk contains only a small fraction ($\sim 10\%$) of the total mass in the computational domain. Hence to a first approximation we can assume that the gas moves in the potential field of the stars and DM halo.

Once the density profile of the gas disk is fixed, its initial rotation curve (RC) is obtained by solving Eq. (2), where the friction force f is set to zero and the time variations are neglected. The resulting initial RC is plotted in Fig. 1, where it reaches a maximum circular velocity of 200 km s^{-1} at $r \approx 3$ kpc. Beyond this maximum, the rotational velocity undergoes a gradual decline. Because the gas surface density has a slowly declining radial profile ($r_{\rm g} = 9$ kpc) and the gas is assumed to be isothermal, the contribution of the pressure gradient in the gas rotation curve is less than 1% everywhere in the disk.

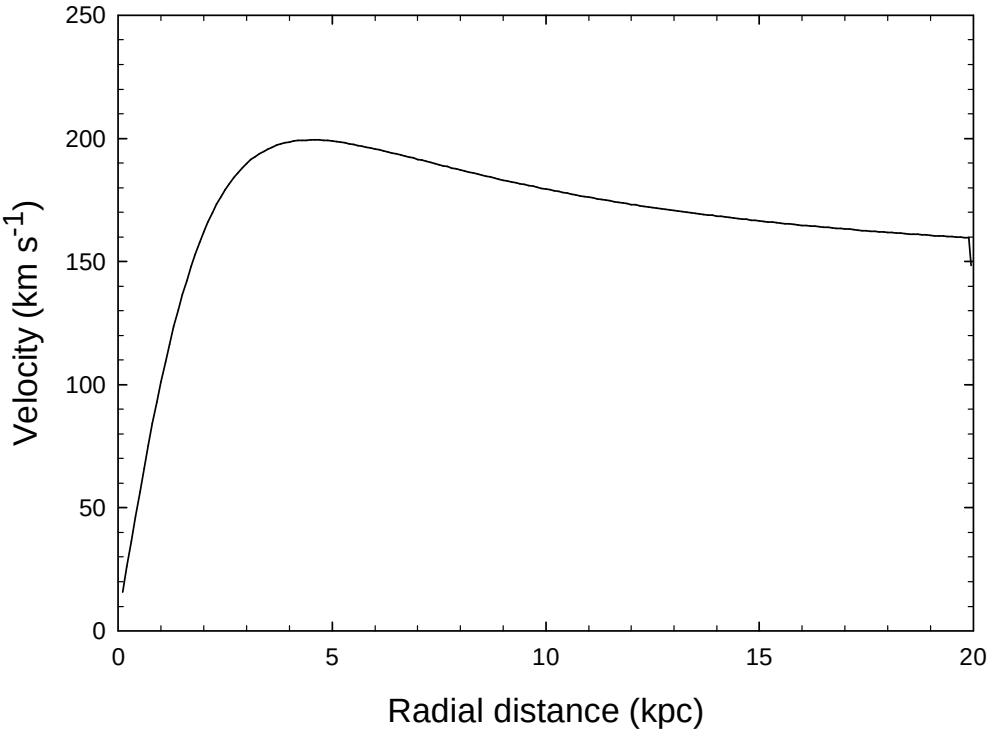

Fig. 1. The initial rotation curve of the gas disk.

2.3 Computational techniques

A set of hydrodynamic equations (1)-(3) in polar coordinates (r, ϕ) is solved using the method of finite-differencing with a time-explicit, operator-split solution procedure (ZEUS-2D) described in detail in Stone and Norman (1992). We use a resolution of 200×200 grid points in a polar computational domain with a radius of 20 kpc. We set a free boundary condition at the outer boundary, i.e. the gas and dust are allowed to flow out freely from the computational domain. The outflowing gas/dust is assumed to be lost by the parent galaxy.

3 Generation of spiral pattern

Once the axisymmetric equilibrium gas disk is constructed, we introduce the non-axisymmetric spiral gravitational potential of the stellar disk Φ_{s2}. The latter is defined in the form of a running spiral density wave (Lin et al., 1969)

$$\Phi_{s2} = -C(r) \cos\left[m(\cot(i) \ln(r/r_{sp}) + \phi - \Omega_{sp} t)\right]. \quad (11)$$

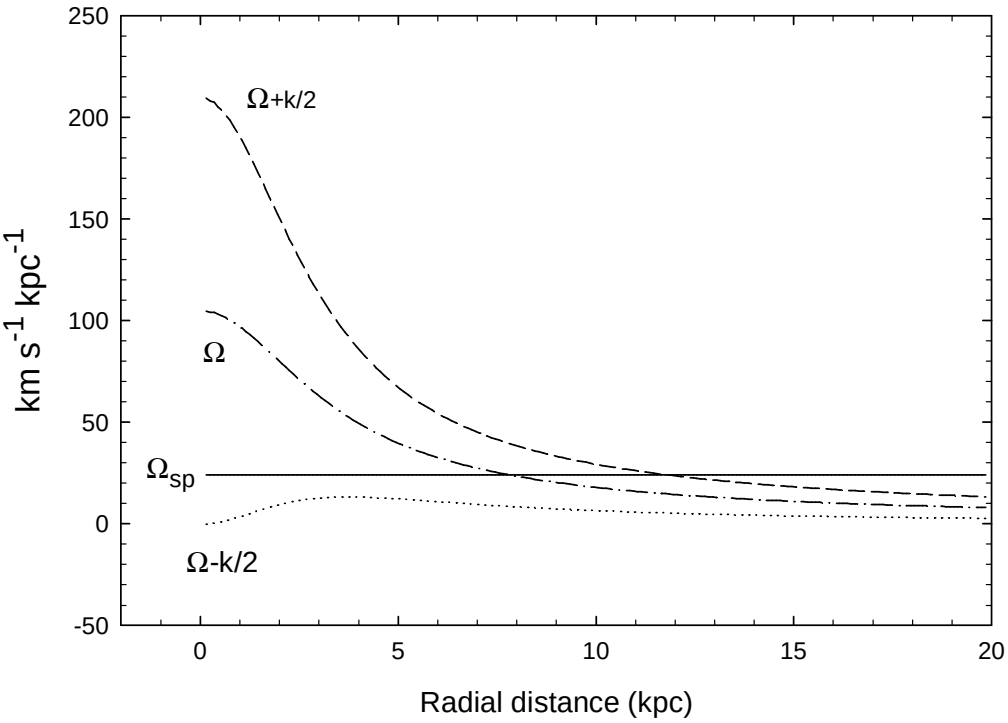

Fig. 2. Behaviour of $\Omega \pm \kappa/2$, where κ is the epicyclic frequency and Ω is the angular velocity of gas. The angular velocity of spiral pattern $\Omega_{\rm sp}$ is shown by the solid line.

Here, $C(r)$ is the amplitude of the spiral gravitational potential, m is the number of spiral arms, i is the pitch angle, $r_{\rm sp}$ is the characteristic winding length of spiral arms, and $\Omega_{\rm sp}$ is the angular velocity of spiral pattern. In the following we adopt $m = 2$, $i = 25^\circ$, $r_{\rm sp} = 6$ kpc, $\Omega_{\rm sp} = 24$ km s^{-1} kpc^{-1}. This choice of $\Omega_{\rm sp}$ places the corotation of the gas disk at ≈ 8.0 kpc and the outer Lindblad resonance at ≈ 12.0 kpc. The inner Lindblad resonance is absent. The behavior of gas angular velocity Ω and $\Omega \pm \kappa/2$ is shown in Fig. 2. According to Kennicutt (1981), a pitch angle of $i = 25^\circ$ is typical for Sc galaxies. The efficiency of radial transport of dust for different pitch angles is discussed in Sect. 5.

The logarithmic spiral defined by Eq. (11) is quickly winding up as $r \to 0$. This may create large gradients of gravitational potential near the origin and lead to serious numerical difficulties. For instance, if the amplitude $C(r)$ is independent of r, than the ratio of maximum non-axisymmetric perturbing force to the total axisymmetric gravity force $\beta(r) = max|\nabla \Phi_{\rm s2}|/(\partial \Phi_{\rm s1}/\partial r + \partial \Phi_{\rm h}/\partial r)$ sharply increases as $r \to 0$. This is illustrated in Fig. 3, where $\beta(r)$ is plotted by the dotted line for $C = 0.005$ (in dimensionless units). The apparent growth of β with radius for $r > 3$ kpc is also unrealistic since the spiral arms are expected to vanish at larger radii. In view of these difficulties, we use a radially dependent amplitude of the form $C(r) = C_0(r)^{\alpha(r)}$. Here,

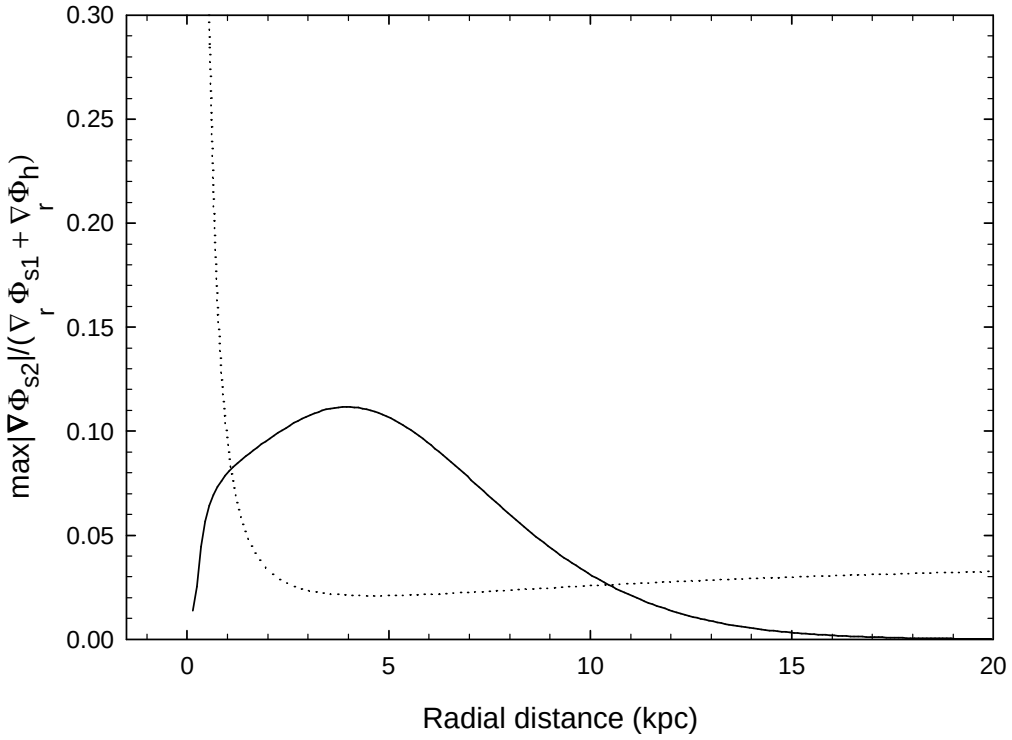

Fig. 3. The ratio of the maximum, non-axisymmetric perturbing force $|\boldsymbol{\nabla}\Phi_{\rm s2}| = [(\partial\Phi_{\rm s2}/\partial r)^2 + (r^{-1}\partial\Phi_{\rm s2}/\partial\phi)^2]^{1/2}$ to the total axisymmetric gravity force $(\partial\Phi_{\rm s1}/\partial r + \partial\Phi_{\rm h}/\partial r)$ as a function of radial distance. The solid and dashed lines are explained in greater detail in the text.

$C_0(r)$ is a linear function of r which has a value of 0 at $r = 0$ kpc (ensuring that $|\boldsymbol{\nabla}\Phi_{\rm s2}|$ diminishes as $r \rightarrow 0$) and attains its maximum value of 0.0045 (in dimensionless units) at $r = 20$ kpc. The exponent $\alpha(r)$ decreases linearly with radius from $\alpha = 2$ at r=0 kpc to $\alpha = -2.1$ at r=20 kpc. The resulting profile of $\beta(r)$ is shown in Fig. 3 by the solid line. Since the non-axisymmetric gravity force scales as $|\boldsymbol{\nabla}\Phi_{\rm s2}| \propto 1/r^{1-\alpha(r)}$, the ratio β increases with radius at $r < 4$ kpc, and decreases at $r \gtrsim 4$ kpc. At the position of corotation $r_{\rm cr} \approx 8$ kpc, β drops by roughly a factor of 2 as compared to its maximum value at $r \approx 4$ kpc and continues to decrease at larger radii. We note that the maximum, non-axisymmetric perturbing force never exceeds 12% of the total axisymmetric gravity force.

The non-axisymmetric part of the stellar gravitational potential $\Phi_{\rm s2}$ is turned on slowly. Specifically, $\Phi_{\rm s2}$ is multiplied by a function $\epsilon(t)$, which has a value of 0 at t=0 and linearly grows to its maximum value of 1.0 at $t \geq 200$ Myr. It takes a few hundred Myr for the gas disk to adjust to the spiral distortion and develop a spiral structure as shown in Fig. 4. The gas spiral pattern (as well as the stellar one) rotates counterclockwise. The position of corotation

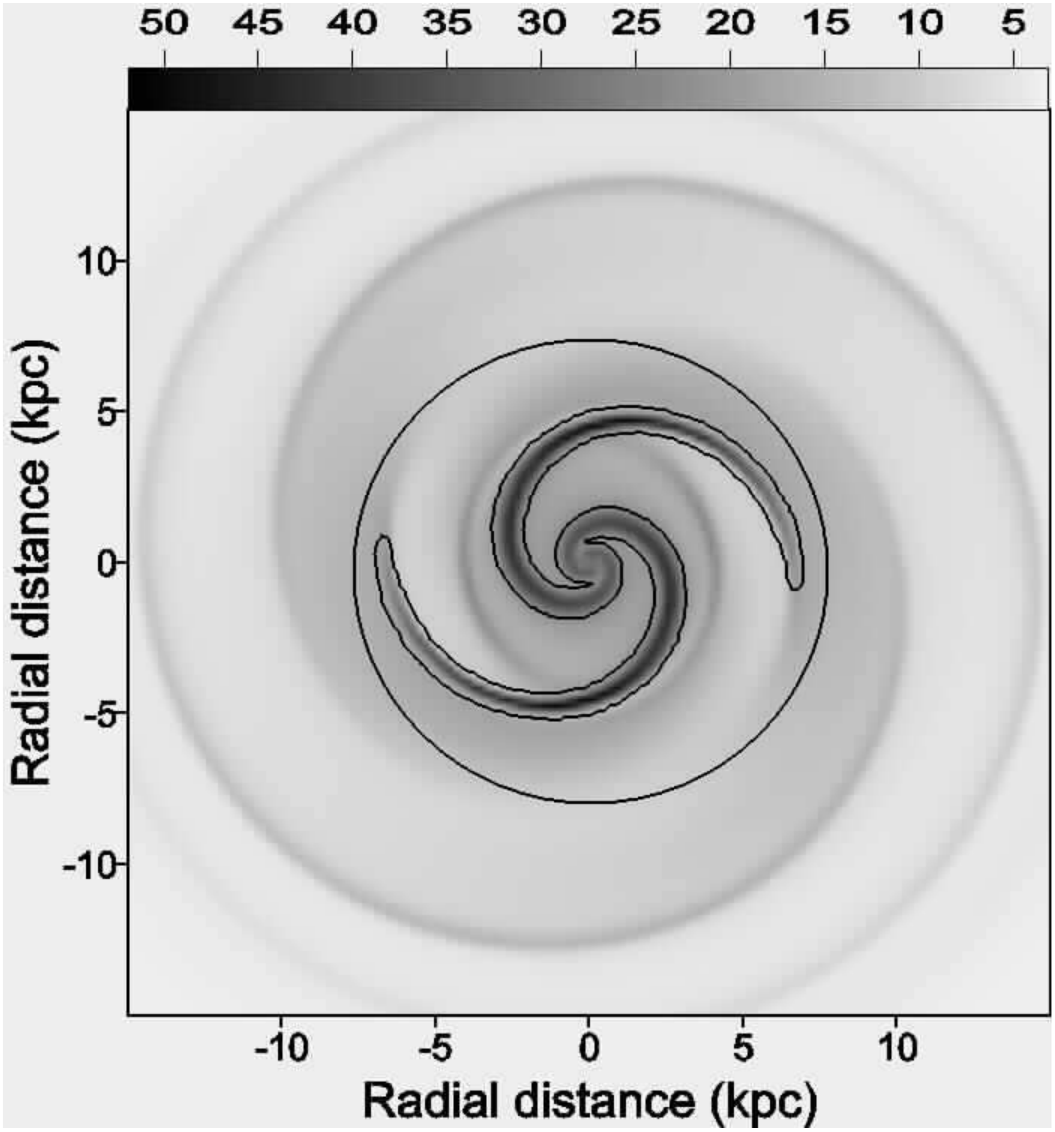

Fig. 4. Gas density distribution at $t = 0.8$ Gyr from the beginning of numerical simulations. The corotation radius is shown by the circle. The scale bar is in $M_\odot$ pc^{-2}. The contour line sketches the region of supercritical gas density (see Sect. 5 for details).

is shown by the circle. The strongest gas response to the underlying stellar spiral density wave is seen inside the corotation circle. However, a weak spiral structure can still be traced outside corotation at radii $r = 10 - 15$ kpc.

4 Trajectories of dust particles

In this section we study the trajectories of single dust particles in the combined gravitational potential of stellar disk and dark matter halo including

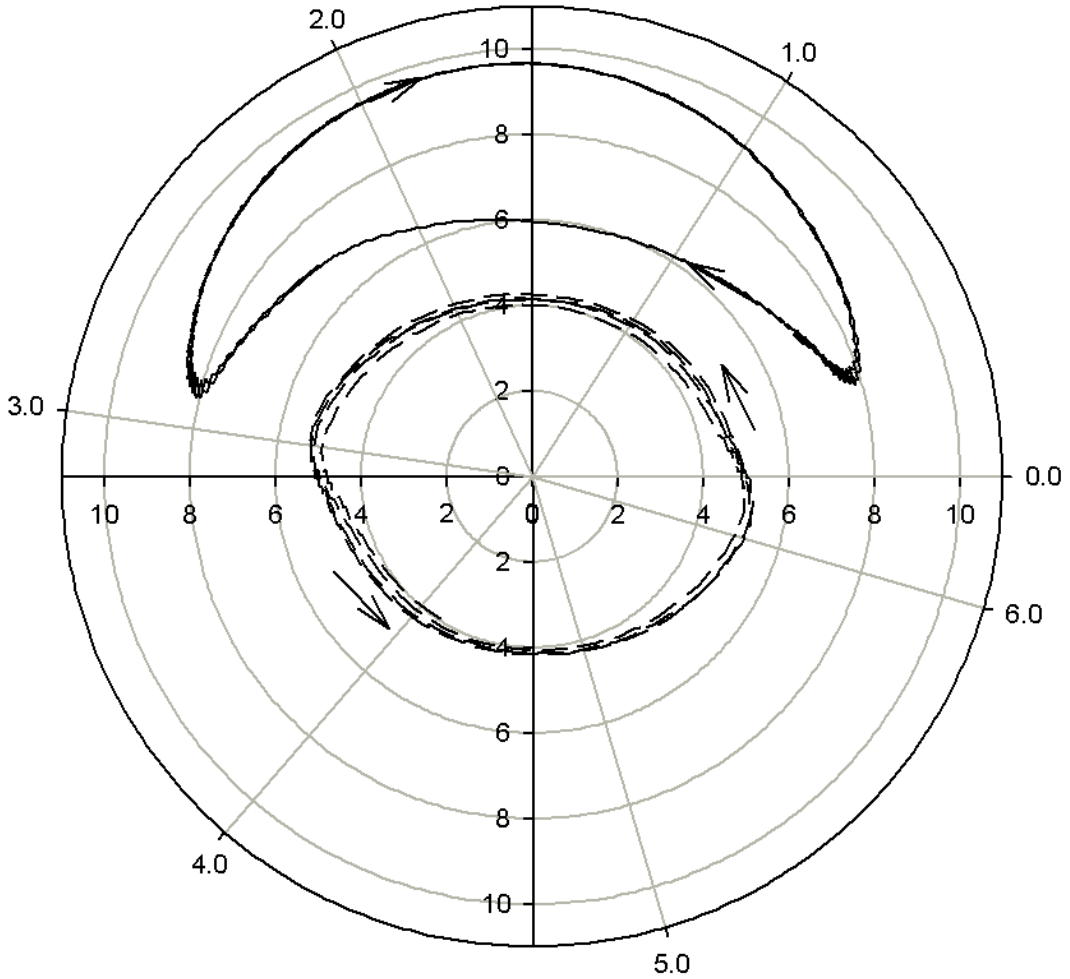

Fig. 5. Polar plot (r, θ) showing trajectories of three test dust particles. The radial distance is in kiloparsecs and the azimuthal angle is in radians. Stellar spiral arms are located along azimuthal angles of 0 and π. The direction of motion of test particles in the frame of reference of stellar spiral arms is indicated by arrows.

the effects of dust-gas friction. The equation of motion of the dust fluid (3) can be obviously reduced to a set of equations of motion for a single dust particle and subsequently solved using the Runge-Kutta scheme. We introduce test dust particles at different radial distances from the galactic centre $r_{\rm d}$ and at different azimuthal angles $\theta_{\rm d}$ with respect to the position of stellar spiral arms. In our simulations, the stellar spiral arms are modeled by the spiral gravitational potential rotating counterclockwise in the laboratory frame of reference. Therefore, the position of stellar spiral arms at any given time is determined as the position of minimum in the spiral gravitational potential defined by Eq. (11). All dust particles are injected at $t = 0.8$ Gyr when the gas spiral structure is fully developed (see Fig. 4), and they are assigned velocities drawn from the parent gas. We followed the trajectories of test dust particles for 2 Gyr.

The phase $(r_{\rm d}, \theta_{\rm d})$ trajectories of three representative dust particles *in the*

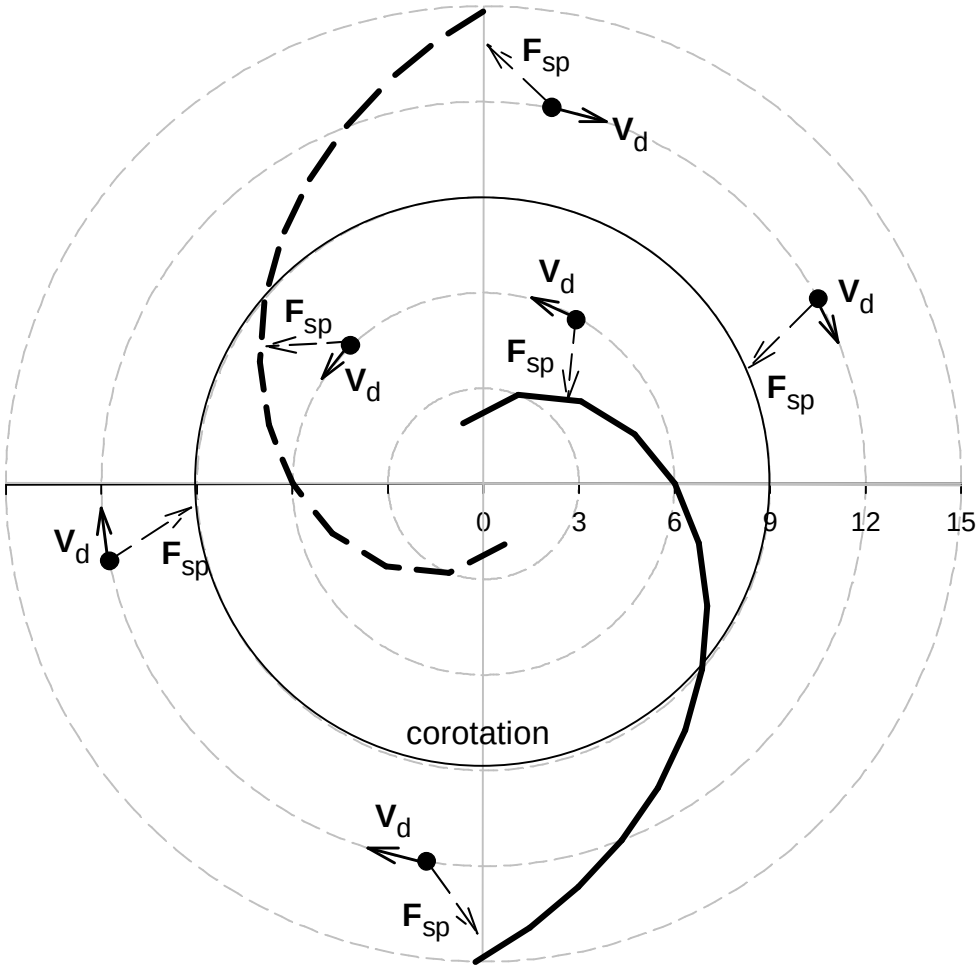

Fig. 6. Schematic description of gravity forces (shown by the dashed arrows) acting on test dust particles from the stellar spiral arms (plotted by thick solid and dashed lines). Velocities of dust particles in the frame of reference of stellar spiral arms are indicated by solid arrows. Two test particles inside corotation and four test particles outside corotation are shown. Arrows are not to scale.

frame of reference of stellar spiral arms are shown in Fig. 5. The stellar spiral arms in Fig. 5 are always located along azimuthal angles $\theta_{\rm sp} = 0$ and π. The dashed line shows the trajectory of a dust particle placed initially at $r_{\rm d}$=5.0 kpc in the arm ($\theta_{\rm d} = 0$; hereafter, particle 1), whereas the solid line gives the trajectory of a dust particle placed initially at $r_{\rm d}$=7.0 kpc in the interarm region ($\theta_{\rm d} = \pi/4$; hereafter, particle 2). Dust particles similar to particle 1 may be injected by supernova explosions which tend to occur near spiral arms. Particle 2 may be created by red giant stars.

It is apparent that the trajectories of particles 1 and 2 are quite different. Particle 1 moves on an elliptical orbit in one direction (counterclockwise), remaining always inside the corotation circle ($r_{\rm cr} \approx 8.0$ kpc). The trajectory

of particle 1 is fairly stable. It comes closer to the origin when traveling between the arms ($\theta_{\rm d} \approx \pi/2$) and it passes through the spiral arms 4 times during 0.65 Gyr. Since dust particles are thought to be destroyed by supernova explosions, such a frequent encounter with the spiral arms implies that particle 1 may not live longer than 0.5 Gyr (although it depends on the covering factor of sufficiently strong shock waves, $v_{\rm SN} \gtrsim 100$ km s^{-1}, generated by supernova explosions (SNe) and propagating perpendicular to the spiral arms). Particle 2 has a stable, kidney-shaped trajectory, which shows an impressive radial migration of ~ 4 kpc, as opposed to only 1 kpc for particle 1. Interestingly, particle 2 is caught between the spiral arms, periodically passing through the corotation circle from the inner part of the disk to the outer part and vice versa. Since particle 2 never encounters the spiral arms during 2 Gyr, it may live significantly longer than particle 1. Dust particles that are born at $\theta_{\rm d} \approx \pi/2$ (i.e. exactly between the spiral arms) but are sufficiently away from the galactic center, move on much more compact orbits as shown by the dotted line in Fig. 5.

To summarize, we find that all particles born at $r < 6$ kpc, i.e. $\gtrsim 2.0$ kpc away from the position of corotation radius $r_{\rm cr} \approx 8.0$ kpc, always stay inside corotation. This is irrespective of their azimuthal angles of birth. Trajectories of those dust particles resemble that of particle 1 shown in Fig. 5 by the dashed line. Such particles often encounter spiral arms and thus may be destroyed in one rotation period by shocks from SNe. The fraction of surviving dust grains is determined by the probability for them to meet a sufficiently strong ($v_s \gtrsim 100$ km s^{-1}) destroying shock wave inside the arm. On the other hand, particles injected near corotation at 6 kpc $\lesssim r < 8.0$ kpc (and sufficiently away from spiral arms) spend most of their lifetime in the interarm region. Therefore, most of these dust particles can survive over the entire migration period in the outer galactic regions.

In the absence of spiral arms, dust particles move on circular orbits determined by the axisymmetric global gravitational potential of a galaxy and the drag force from the gas disk. When the non-axisymmetric spiral gravitational potential is introduced, dust particles move on various non-circular orbits as shown in Fig. 5. In order to understand the origin of such non-circular orbits, we consider the influence of a non-axisymmetric spiral gravity force on the motion of dust particles. The gravity force of spiral arms acting on moving particles is schematically plotted in Fig. 6 by the dashed arrows. Six particles are presented; two particles inside the corotation circle and four particles outside the corotation circle. The direction of motion of dust particles *in the frame of reference of the spiral pattern* is shown by the solid arrows. Two spiral arms are schematically shown by the solid and dashed lines. A moving dust particle may see the nearest spiral arm as either convex or concave. If the dust particle is closer to the concave spiral, the latter acts to increase (on average) the radial distance of the particle due to its gravitational drag.

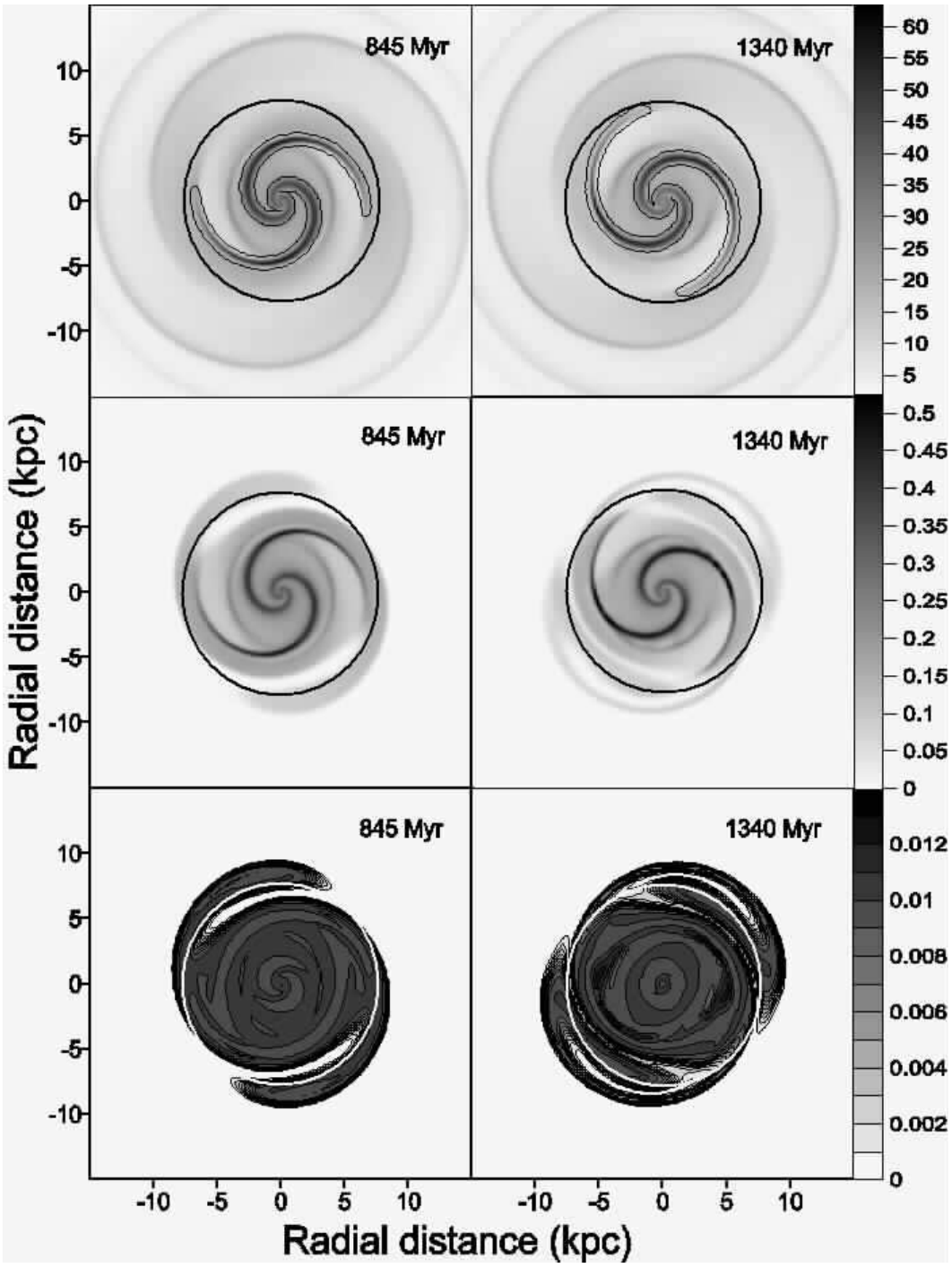

Fig. 7. Gray-scale images of the gas distribution (the upper panels), dust distribution (the middle panels) and the dust-to-gas ratio (lower panels). The elapsed time is indicated in each panel. The position of corotation of the gas disk is outlined by the circle. The scale bars in the upper and middle panels give the column density in $M_\odot$ pc^{-2}

On the contrary, if the dust particle is closer to the convex spiral, the latter tends to decrease the radial distance of the particle. If we now recall that the trailing spiral arms in Fig. 5 are located along the azimuthal angles 0 and π and rotate counterclockwise, then the effect of gravitational drag from the spiral arms becomes clearly evident in the trajectories of dust particles. For instance, when dust particles are in the first quadrant, they are attracted by the convex spiral located at $\theta_{\rm sp} = 0$. As a consequence, the radial position of these particles decreases. When dust particles enter the second quadrant, their motion is controlled by the concave spiral located at $\theta_{\rm sp} = \pi$ and their radial position increases. Therefore, the trajectories of dust grains may be sensitive to the pitch angle of stellar spiral arms. The maximum radial migrations of dust grains are expected for a pitch angle of 45°.

The action of the friction force is more difficult to assess. The friction between dust and gas may help reverse the direction of motion of a dust particle (with respect to the spiral arms) when it passes through corotation. Indeed, when the dust particle is inside the corotation circle, its velocity is larger than that of spiral arms (the same is true for the gas in general). After passing through corotation, the dust particle enters the region which is characterized by a smaller velocity than that of spiral arms. Therefore, we may expect that the friction between gas and dust would act to equalize the velocities of dust and gas, and thus decelerate the dust particles. This would eventually reverse their direction of motion with respect to the spiral arms as seen in Fig. 5 for particle 2.

5 Response of dust to the stellar spiral density wave

In this section we study how dust responds to the imposed spiral disturbance. The dominant sources of dust formation in disk galaxies are stellar winds from late-type giant and supergiant stars, supernova explosions, and growth of pre-existing grains in dense $n \gtrsim 10^3$ cm^{-3} molecular clouds (Dwek, 1998). All of these sources are mainly located inside the corotation circle. Indeed, the strongest gas response to the stellar spiral density wave in Fig. 4 is obviously seen inside corotation. We compute the critical density for star formation as defined by the Toomre criterion (Kennicutt, 1989)

$$\Sigma_{\rm crit}^{\rm Toomre} = \frac{0.7\, c_{\rm s}\, \kappa}{\pi\, G}, \tag{12}$$

where κ is the epicyclic frequency, and the shear criterion (Martin and Kennicutt, 2001)

$$\Sigma_{\rm crit}^{\rm shear} = \frac{2.5 A_{\rm sh}\, v_{\rm s}}{\pi G}, \tag{13}$$

where $A_{\rm sh} = -0.5\, r\, {\rm d}\Omega/{\rm d}r$ is the local shear rate (the Oort constant). The contour line in Fig. 4 traces the region of supercritical density with $\Sigma_{\rm g} > \min(\Sigma_{\rm crit}^{\rm Toomre}, \Sigma_{\rm crit}^{\rm shear})$ which is evidently localized inside corotation. Although the gas density outside corotation may occasionally become supercritical (not shown in Fig. 4) especially along the outer diffuse gas spirals, a lower gas density and higher temperature as compared to the inner region can work against star formation in that region. We thus conclude that most of star formation in our model galaxy is localized within the corotation circle. The radial scale length of our old stellar disk is $r_{\rm s} = 3$ kpc which also implies that most of low to intermediate mass stars that are capable of producing dust are confined within the corotation circle.

We instantaneously inject $3.4 \times 10^7\ M_\odot$ of dust mass inside the corotation circle ($r < 7.8$ kpc) and then determine the fraction of dust that can move outside corotation. In the present simulations, the dust particles are injected at $t = 0$ Myr when a spiral structure in the gas disk has not yet developed. We also tried to introduce dust at t=800 Myr (when the gas spirals are fully developed) and confirmed that the time of dust injection has little influence on dust dynamics. The spatial distribution of injected dust is such that the dust-to-gas ratio $\gamma = 0.01$ inside corotation, and $\gamma = 0$ outside corotation. The velocity of injected dust is equal to that of the gas. A conservative estimate of dust-to-gas mass ratio in the solar neighborhood gives an average value of $\gamma = 0.006$ ranging from 0.002 up to 0.04 in H_2 regions (Spitzer, 1978).

The upper and middle panels in Fig. 7 show two snapshots of the evolution of the gas and dust surface densities, respectively, whereas the lower panels give the dust-to-gas mass ratio. The numbers in each panel indicate the elapsed time since the beginning of the simulation. The circle indicates the position of corotation of the gas disk. A strong spiral response to the stellar density wave develops in the dust disk after approximately 3 revolution periods of our model galaxy. The dust density closely follows that of gas in the inner regions of our model galaxy. Small radial and azimuthal variations of the dust-to-gas ratio around the initial value 0.01 are indicative of a dominant role of frictional force in the dynamics of dust in the inner 5 kpc. This is in agreement with the results of Sect. 4 where we have found that dust particles born in the inner 5 kpc move on fairly stable elliptical orbits around the galactic center. At larger radii 6 kpc $\lesssim r < 8.0$ kpc, however, significant variations of γ become evident. There are regions near corotation that are completely devoid of dust, even though the initial dust-to-gas ratio is 0.01. A noticeable portion of dust is

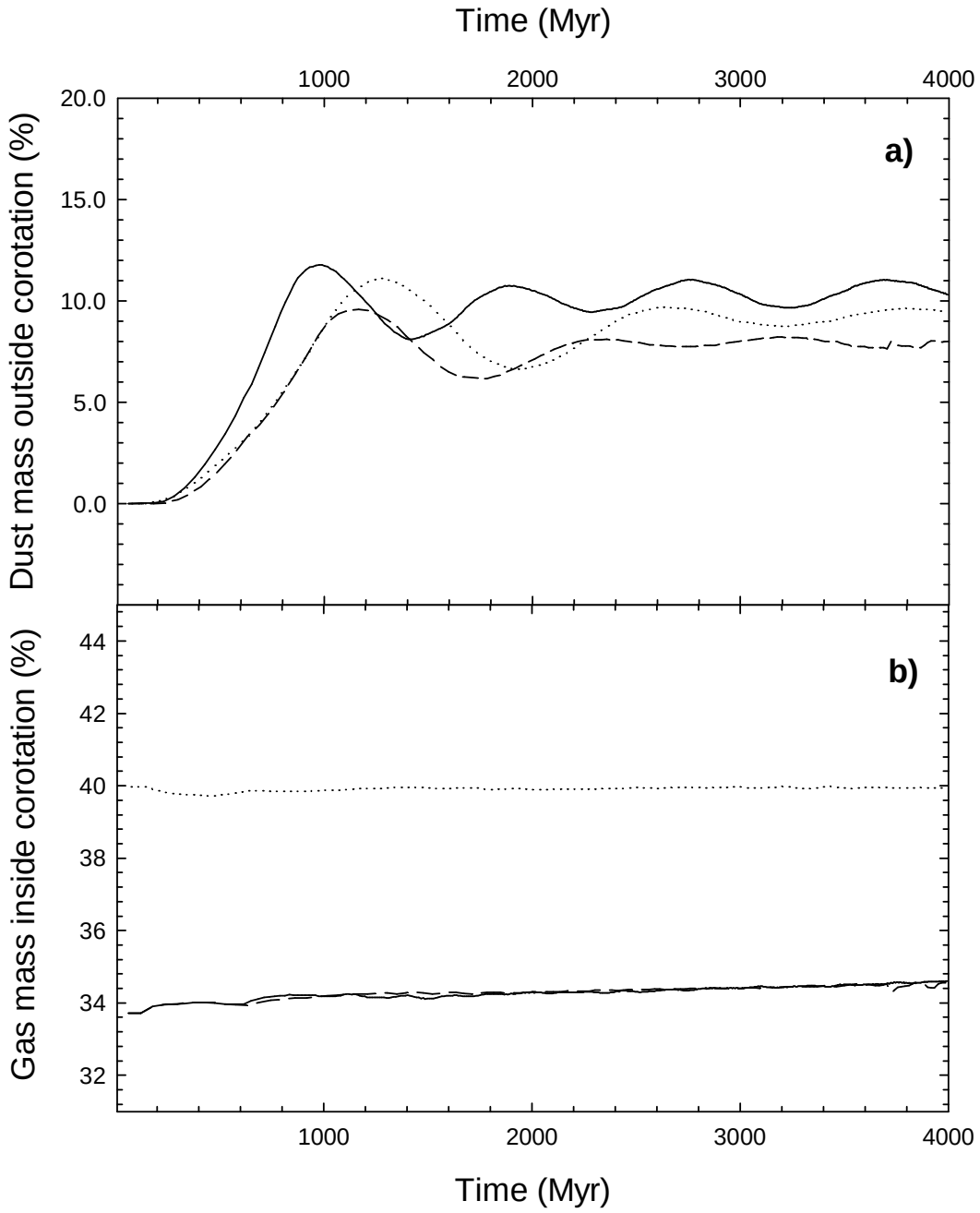

Fig. 8. **a)** Dust mass ouside corotation as a percentage of the total dust mass. The solid and dashed lines correspond to the models with pitch angles of stellar spiral density wave $i = 25°$ and $i = 15°$, respectively. The dotted line gives the dust mass outside corotation for a lower rotation frequency of stellar spirals $\Omega_{\rm sp} = 21$ km s^{-1} kpc^{-1}. **b)** Gas mass inside corotation as a percentage of the initial total gas mass. The solid, dashed, and dotted lines correspond to the same models as in the upper panel. The difference in the values of the gas fraction inside corotation for $\Omega_{\rm sp} = 21$ km s^{-1} kpc^{-1} and $\Omega_{\rm sp} = 24$ km s^{-1} kpc^{-1} is due to the different positions of the corotation radius in the two cases.

observed outside corotation. This dust tends to form into diffuse outer spiral arms, which appear to be a smooth extension of the inner dust spiral arms and can be traced up to $r = 10$ kpc. The dust-to-gas ratio in the outer dust arms is not dissimilar to that of the inner $r < 5$ kpc region. We thus conclude that the perturbing force of stellar spirals starts to play an important role in the dust dynamics near corotation resulting in an outward radial transport of dust. If we now identify the regions of supercritical gas density by contour lines in the upper panels of Fig. 7, than it becomes evident that the dust component can be found as far as 4-5 kpc from the sites of active star formation.

The solid line in Fig. 8a gives the dust mass outside corotation (as a percentage of the total dust mass) versus time elapsed since the injection of dust. Approximately 10% of the initial injected dust mass is transported outside corotation during 1 Gyr. This implies that the dust transport rate is $\dot{M} = 3.8\ M_{\odot}\ \mathrm{Myr}^{-1}$. At later times, the amount of transported dust varies around $\approx 10\%$ of the total dust mass. These variations are mainly due to dust particles born inside the corotation circle in the interarm region, where they are trapped into periodic orbits as shown by solid and dotted lines in Fig.5. We conclude that only a (small) fraction of dust particles (approximately 10% by mass) injected instantaneously inside the corotation circle can move to the outer regions, while the rest is confined in the inner galaxy. As a consequence, the radial transport of an instantaneously injected portion of dust terminates after ≈ 1 Gyr.

The spiral stellar density wave considered so far has a pitch angle of $i = 25^{\circ}$. This is typical for Sc galaxies (Kennicutt, 1981). The efficiency of outward radial transport of dust may depend on the openness of stellar spiral arms. To test this conjecture, we explored a series of models with different pitch angles. The dashed line in Fig. 8 shows the the dust mass outside corotation as a percentage of the total dust mass for the stellar spiral with a pitch angle $i = 15^{\circ}$. Roughly 8% of the injected dust mass is pushed outside corotation, as compared to $\approx 10\%$ for $i = 25^{\circ}$. This indicates that the efficiency of outward radial transport of dust drops by roughly 2%. We expect that the radial transport of dust by spiral stellar density waves may becomes inefficient for very tightly wound spirals with a pitch angle $i \lesssim 5^{\circ}$. Our simulations have also shown that the efficiency of outward transport of dust is weakly sensitive to the angular velocity Ω_{sp} of stellar spirals. For instance, a stellar spiral with $\Omega_{\mathrm{sp}} = 21$ km s^{-1} kpc^{-1} can transport roughly 1% less dust (see the dotted line in Fig. 8) than a spiral with $\Omega_{\mathrm{sp}} = 24$ km s^{-1} kpc^{-1}. We note that the corotation radius for $\Omega_{\mathrm{sp}} = 21$ km s^{-1} kpc^{-1} is at 8.8 kpc.

The solid line in Fig. 8b shows the gas mass inside corotation as a percentage of the total initial gas mass. [2] It is evident that the gas (contrary to the dust) does

[2] Due to the imposed outflow outer boundary condition, we cannot reliably calculate the gas mass outside corotation because its value can be affected by the

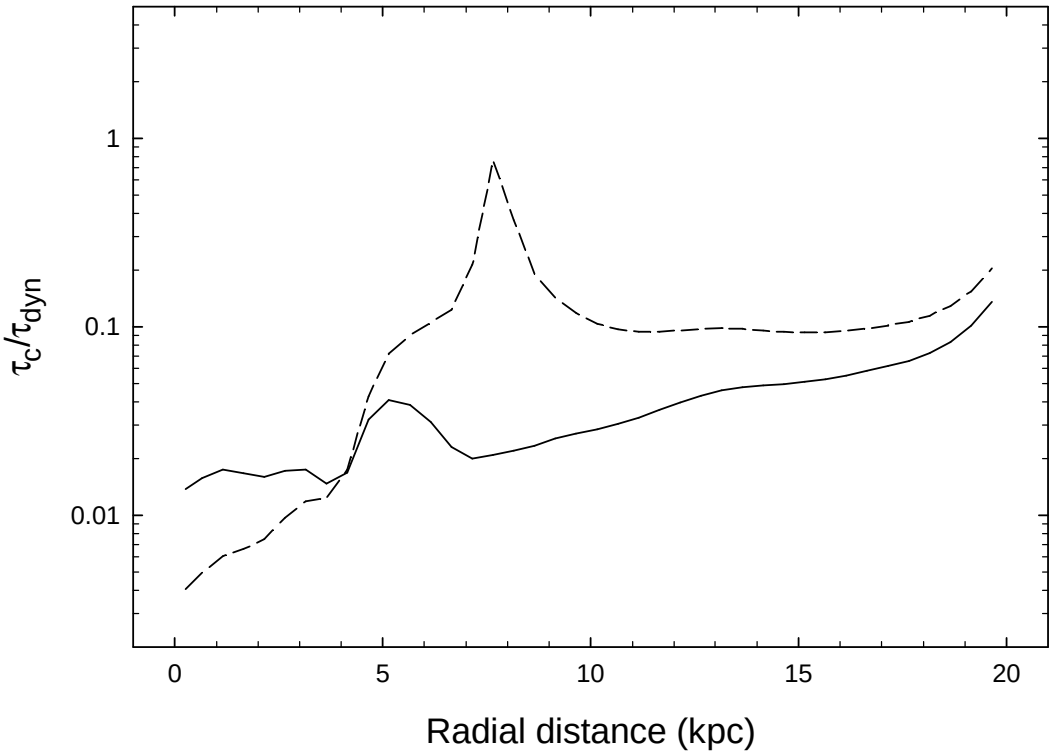

Fig. 9. The ratio of the frictional timescale $\tau_{\rm c}$ to the dynamical timescale $\tau_{\rm dyn}$ as a function of radius at $t = 1340$ Myr. The solid and dashed lines show $\tau_{\rm c}/\tau_{\rm dyn}$ for the dynamical timescale defined as $\tau_{\rm dyn} = \Omega_{\rm d}^{-1}$ and $\tau_{\rm dyn} = |\Omega_{\rm d}^{-1} - \Omega_{\rm sp}^{-1}|$, respectively. The detailed explanation is given in the text.

not exhibit a noticeable radial migration. A very weak inward radial transport ($\sim 1\%$ by mass) is seen for $\Omega_{\rm sp} = 24$ km s^{-1} kpc^{-1}, and it becomes negligible for $\Omega_{\rm sp} = 21$ km s^{-1} kpc^{-1}. We attribute this difference between the gas and dust radial transport rates to the restoring force of the pressure gradients which are always present in the warm ($T_{\rm g} \sim 10^4$ K) gas. The warm gas resists radial redistribution by creating additional pressure gradients which act to restore the initial centrifugally balanced configuration. The dust, however, is cold and it can easily flow in the radial direction provided that the coupling between dust and gas is not very strong.

To determine the main cause of the radial transport of dust, we compute the quantity $\tau_{\rm c}/\tau_{\rm dyn}$ (averaged over 0.5 kpc radial annuli). This quantity as a function of radius is shown by the solid line in Fig. 9 at the time when the gas spiral is fully developed. The collisional timescale $\tau_{\rm c}$ of energy and momentum exchange between the dust and gas particles is defined in Eq. (4). The local dynamical timescale is defined as $\tau_{\rm dyn} = \Omega_{\rm d}^{-1} = r/v_{{\rm d},\phi}$, where $v_{{\rm d},\phi}$ is the azimuthal component of dust velocity $\boldsymbol{v}_{\rm d}$. If $\tau_{\rm c} \ll \tau_{\rm dyn}$ the dust is expected to be strongly frictionally coupled to the gas and to essentially track the gas

gas that leaves the computational area. The dust, however, never reaches the outer boundary.

motion. Figure 9 shows that τ_c is a factor of $0.01-0.1$ smaller than τ_{dyn}, which implies a strong frictional coupling betwen dust and gas. However, judging from the bottom panels of Fig. 7, it would appear that the dust does not follow exactly the gas motion in the region near corotation. The reason is that the dust particles have natural resonant frequencies near corotation (remember that corotation determines the position of resonance in gas/dust orbits). If the gravitational field generated by spiral structure perturbs a dust particle's orbit at or near its resonant frequency, then the responce of the orbit will be large, even when the perturbing field is weak and/or the frictional coupling is strong. To investigate this effect, we re-define the local dynamical time as $\tau_{dyn} = |\Omega_d^{-1} - \Omega_{sp}^{-1}|$ and plot the corresponding quantity τ_c/τ_{dyn} in Fig. 9 by the dashed line. It is now evident that the frictional coupling between dust and gas is much weaker near corotation. This is consistent with the trajectories of dust particles found in Sect. 4 – only the dust particles that are born near corotation show substantial radial migration.

Another source of uncertainty in our simulations is the friction coefficient A, which we have adopted in the form of Eq. (4) to simplify the computations. As is pointed out in Sect. 2.1, the total stellar+gas surface density $\Sigma_s + \Sigma_g$ (instead of simply gas surface density, Σ_g) should appear in the definition of the gas vertical scale height

$$z_0 = \frac{c_s^2}{\pi G(\Sigma_s + \Sigma_g)}, \tag{14}$$

which may considerably increase the value of A. The uncertainity in the value of Σ_s (we do not explicitly follow the evolution of the stellar disk) works against this re-definition of z_0 in our simulations. In order to estimate the effect that the increased surface density of gravitating matter in Eq. (14) may have on the radial transport of dust particles, we notice that in the region of interest near corotation the ratio of stellar-to-gas surface densities is usually in the $1.5-15$ range. Therefore we performed a test run in which A was defined by Eq. (4), but was later multiplied by a factor of 10. The efficiency of outward radial transport of dust increased by less than 1%. In another test, A is decreased by a factor of 10, and the efficiency of outward radial transport of dust is dropped by approximately 1%. We conclude that an order of magnitude variation in A has a minor effect on the efficiency of radial transport of dust. This reinforces a previous conclusion: the resonant region near corotation, where $\Omega_d \approx \Omega_{sp}$, and the collisional drag force is dynamically less important than the spiral gravitational field, determines the radial migration of dust.

6 Dust destruction

In this section we study the effect of dust destruction by SNe on the efficiency of radial transport of dust in spiral galaxies. The dust grain destruction by SNe is the most important mechanism for cycling the dust back to the gas phase. The dust destruction rate can be determined as (Dwek, 1998)

$$D_{\rm d}(r,\phi,t) = m_{\rm dest}(r,\phi,t)\,\nu(r,\phi,t). \tag{15}$$

Here, $\nu(r,\phi,t)$ is the supernova rate per unit area and $m_{\rm dest}(r,\phi,t)$ is the mass of dust that is destroyed by a single SN expanding at location (r,ϕ) and time t. Only SN remnants with velocities exceeding 100 km s^{-1} can efficiently destroy dust grains. Therefore, the value of $m_{\rm dest}(r,\phi,t)$ is usually estimated from the relation $m_{\rm dest}/M_{\rm d} = \epsilon M_{\rm g}^{100}/M_{\rm g}$, where $M_{\rm g}^{100} = 3.8\times10^3\ M_\odot$ (Lisenfeld and Ferrara, 1998) is the mass of a remnant accelerated to velocities > 100 km s^{-1} by the blast. This relation simply states that the fraction of destroyed dust (by mass) within a computational cell is directly proportional to the fraction of accelerated remnant mass. The efficiency of dust destruction is $\epsilon \sim 0.1$ (McKee, 1989).

The SN rate per unit area is defined as

$$\nu(r,\phi,t) = \frac{\int_{9M_\odot}^{m_{\rm up}} \Sigma_{\rm SFR}(r,\phi,t-\tau(m))\,m^{-\alpha}\,dm}{\int_{m_{\rm low}}^{m_{\rm up}} m^{1-\alpha}dm}, \tag{16}$$

where $\Sigma_{\rm SFR}$ is the star formation rate per unit area, α is the slope of initial mass function (IMF), $\tau(m)$ is the lifetime of a star of mass m, $m_{\rm low}$ and $m_{\rm up}$ are the lower/upper cutoff masses, respectively. In practice, we approximate the integral in Eq. (16) by the sum with a mass discritization $dm = 1\ M_\odot$.

Observations of both normal and starburst disk galaxies suggest that on the scales of a few kiloparsecs star formation may be represented by a Schmidt law (Kennicutt, 1998)

$$\Sigma_{\rm SFR}\ \left(\frac{M_\odot}{\rm yr\ kpc^2}\right) = 2.5\times10^{-4}\ \Sigma_{\rm g}^{1.5}\ \left(\frac{M_\odot}{\rm pc^2}\right). \tag{17}$$

We modify the star formation law (17) by assuming that star formation is suppressed when $\Sigma_{\rm g} < min(\Sigma_{\rm crit}^{\rm Toomre}, \Sigma_{\rm crit}^{\rm shear})$.

Often, the instantaneous recycling approximation is used to solve Eq. (15), which neglects the time delay that enters Eq. (15) through the SN rate ν.

However, we follow a more accurate approach and form stellar clusters each Myr according to the star formation law (17). Stellar clusters are assigned positions and velocities drawn from the parent gas and are evolved as collisionless particles in the combined gravitational potential of the halo and stellar disk. The local self-gravity among stellar clusters is neglected. Since each stellar cluster carries information on the star formation rate at the time of its birth, the supernova rate $\nu(r,\phi,t)$ and the dust destruction rate $D_{\rm d}(r,\phi,t)$ in each computational cell (r,ϕ) at a time t can be easily obtained. This approach was successfully applied by Vorobyov (2003) to model the $H\alpha$ luminosity in ring galaxies. We use the Salpeter IMF with $\alpha = 2.35$ and lower/upper cutoff masses $m_{\rm low} = 0.5\ M_\odot$ and $m_{\rm up} = 40\ M_\odot$, respectively.

We modify the hydrodynamic equations (1)-(3) of our gas+dust system to take into account star formation and dust destruction. The continuity equations for the gas and dust become

$$\frac{\partial \Sigma_{\rm g}}{\partial t} + \boldsymbol{\nabla} \cdot (\Sigma_{\rm g}\, \boldsymbol{v}_{\rm g}) = S_{\rm g} - D_{\rm g}, \tag{18}$$

$$\frac{\partial \Sigma_{\rm d}}{\partial t} + \boldsymbol{\nabla} \cdot (\Sigma_{\rm d}\, \boldsymbol{v}_{\rm d}) = -D_{\rm d}. \tag{19}$$

The resulting momentum equations are

$$\frac{\partial}{\partial t}\Sigma_{\rm g}\boldsymbol{v}_{\rm g} + (\boldsymbol{v}_{\rm g}\cdot\boldsymbol{\nabla})\Sigma_{\rm g}\boldsymbol{v}_{\rm g} = -\Sigma_{\rm g}\boldsymbol{\nabla}\Phi_{\rm s1,s2,h} - \boldsymbol{\nabla}P_{\rm g} + \Sigma_{\rm d}\boldsymbol{f} + \boldsymbol{v}_{\rm g}(S_{\rm g} - D_{\rm g}), \tag{20}$$

$$\frac{\partial}{\partial t}\Sigma_{\rm d}\boldsymbol{v}_{\rm d} + (\boldsymbol{v}_{\rm d}\cdot\boldsymbol{\nabla})\Sigma_{\rm d}\boldsymbol{v}_{\rm d} = -\Sigma_{\rm d}\boldsymbol{\nabla}\Phi_{\rm s1,s2,h} - \Sigma_{\rm d}\boldsymbol{f} - \boldsymbol{v}_{\rm d}D_{\rm d}. \tag{21}$$

We have rewritten equations of motion in the form of momentum equations for $\Sigma\,\boldsymbol{v}$ which are appropriate for the system with sources and sinks. Star formation depletes the gas reservoir of our model galaxy and is taken into account by the sink term $D_{\rm g} = \Sigma_{\rm SFR}$ in Eqs. (18) and (20). The gas is returned to the system with supernova explosions and quiet mass loss of intermediate and low mass stars. Since we do not use a multiphase description of the interstellar medium, the ejected hot gas is directly transformed into a warm ($T \sim 10^4$ K) phase. The rate of gas ejection per unit area is determined by

$$S_{\rm g} = \frac{\int\limits_{m_{\rm low}}^{m_{\rm up}} g(m)\, \Sigma_{\rm SFR}(r,\phi,t-\tau(m))\, m^{-\alpha}\, dm}{\int\limits_{m_{\rm low}}^{m_{\rm up}} m^{1-\alpha} dm}, \tag{22}$$

where $g(m)$ denotes the gas mass ejected by a star of mass m (Köppen and Arimoto, 1991). We found it computationally prohibitive to compute accurately (i.e. by taking into account the time delay $\tau(m)$ in Eq. [22]) the gas ejection rate by stellar clusters on a time scale of interest (a few Gyr). Therefore, for the stellar clusters older than 100 Myr, the instantaneous recycling approximation is assumed by neglecting the time delay in Eq. (22). These stellar clusters instantaneously release all gas that can be produced by the $0.5 - 5\ M_{\odot}$ stars. Further dynamical evolution of such clusters is not computed.

We study the effect of dust destruction on the radial transport of dust using a prototype model in which the spiral density wave has a pitch angle $i = 25^{\circ}$ and angular velocity $\Omega = 24$ km s^{-1} kpc^{-1}. This model was studied in detail in Sect. 5 where we neglected the effect of dust destruction. It was shown there that about 10% of dust by mass injected instantaneously inside the corotation circle can be transported outside this region by the gravitational drag associated with spiral density waves. We reproduce this result in Fig. 10a by the dashed line, and the solid line gives the dust mass outside corotation as a percentage of the initial total dust mass when dust destruction is taken into account. As is seen, supernova explosions have a minor effect on the radial transport of dust, decreasing the relative amount of dust outside corotation by only 2% when compared to the model without dust destruction. It is worth noting that inside corotation the destruction of dust by supernova explosions is efficient. Indeed, the dashed-dotted and dotted lines in Fig. 10b show the dust mass inside corotation as a percentage of the initial total dust mass when dust destruction is taken and not taken into account, respectively. Approximately 15% of the instantaneously injected dust mass is left inside corotation after 2 Gyr. Given that another 10% has been transported outside corotation, SNe have destroyed about 75% of the injected dust mass during 2 Gyr. In Sect. 5 we argued that the ultimate fate of dust grains would depend on their place of birth. The simulations discussed in this section reinforce our earlier conclusion. In our model dust grains are formed inside the corotation circle at $r_{\rm cr} \approx 8$ kpc. The dust grains that are born in the inner 6.0 kpc circle (by implication they constitute the majority of the total dust mass) move on elliptic orbits periodically crossing the spiral arms and will be inevitably destroyed by supernova explosions after several revolution periods. However, the dust grains that are born in the 6 kpc $\lesssim r < 8$ kpc annulus and sufficiently away from spiral arms (by implication they constitute the minority of the total dust mass) manage to survive the destructive effect of supernova explosions during many revolution periods of our model galaxy. These dust grains may move on orbits similar to those shown in Fig. 5 by the solid and dotted lines, circulating between the spiral arms (but never crossing them) and periodically traveling in and out of the corotation circle. We conclude that a (small) portion of dust grains may survive the destructive effect of SNe during many (> 10) revolution periods of a spiral galaxy.

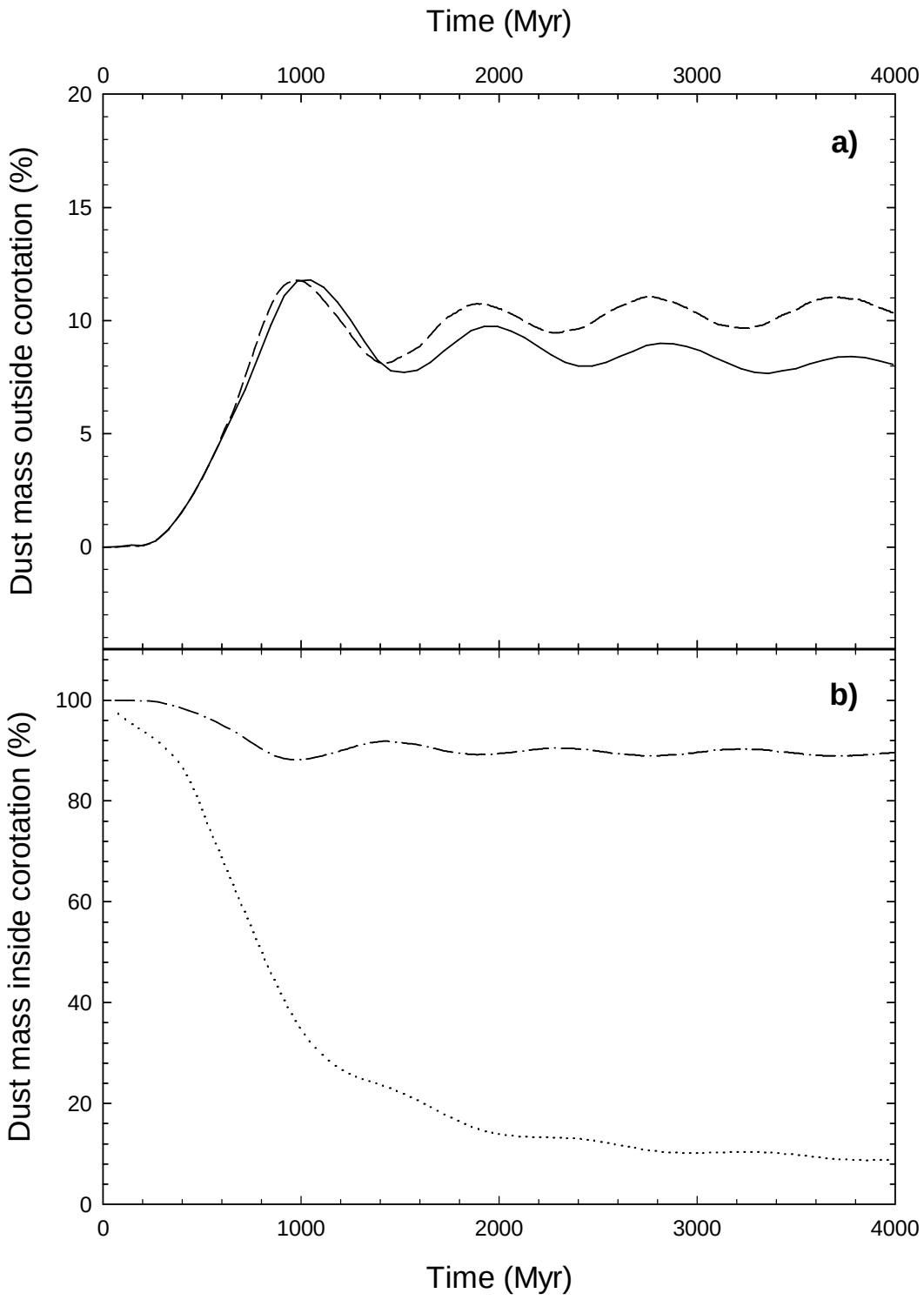

Fig. 10. **a)** Dust mass outside and **b)** inside corotation as a percentage of the total initial dust mass. The solid and dashed lines show the relative dust mass outside corotation in the models with and without dust destruction, respectively. The dotted and dotted-dashed lines give the relative dust mass inside corotation in the models with and without dust destruction, respectively.

7 Summary

In this paper we study the outward radial transport of interstellar dust grains which is connected with the perturbation of circular motions caused by spiral stellar density waves in disk galaxies. We consider a model spiral galaxy in which star formation (and, by implication, dust formation) is localized within the corotation circle. We find that the combined action of the gravity force of spiral stellar density waves and the drag force between the gas and dust components imparts to dust particles a radial velocity component, and thus can evacuate dust outward. We conclude that:

1. Dust grains that are formed inside corotation can be transported to a distance that exceeds the corotation radius by roughly 25%. In particular, if corotation is located at $r_{\rm cr} = 8.0$ kpc, dust grains formed inside the 6 kpc $\lesssim r <$ 8.0 kpc annulus can travel to distances as large as 10 kpc in roughly 1.0 Gyr. This is approximately an order of magnitude faster that can be provided by the interstellar turbulence.

2. A fraction of dust grains can be trapped into the interarm region, and thus can escape a hostile environment from supernova explosions acting mostly in the spiral arms. These grains form diffuse spiral arms which extend 4-5 kpc from the sites of active star formation. Dust particles that cross the spiral arms during their drift outward can survive if they do not meet strong shocks from SNe while passing through the arm.

3. In the model that considers instantaneous dust injection, about 10% of dust by mass is evacuated outside the corotation circle in roughly 1.0 Gyr. One can assume that continuous injection will result in the same percentage of evacuated dust. The efficiency of outward radial dust transport is weakly sensitive to the rotation speed of stellar spirals, but it may be considerably reduced for very tightly wound spirals with a pitch angle $i \lesssim 5^\circ$. Dust destruction by supernova explosions has only a minor effect on the efficiency of outward radial transport of dust by spiral density waves, which decreases the relative amount of transported dust mass by $\sim 2\%$. A (small) portion of dust grains may survive the destructive effect of SNe during many (> 10) revolution periods of a spiral galaxy.

4. Our modeling shows that the dust-to-gas ratio in the region near corotation (± 2 kpc) can vary substantially over the scales comparable to the thickness of spiral arms, ~ 1 kpc. Possible observations of such variations would be suggestive of the proposed mechanism of radial dust transport.

In our model we neglected the fact that charged dust grains are strongly coupled to the magnetic field – the gyration frequency for a typical grain with radius $a \sim 0.1\mu$m and grain charge $Z \sim 100$ is of $\omega_B \sim 10^{-10}$ Hz. We

expect that in more realistic models, where the magnetic field is permanently regenerated by a turbulent dynamo, dust particles will be involved in both the turbulent diffusive motions and regular flow, and the overall picture will remain qualitatively similar to that described above. We leave this issue for further study.

We should mention that the interaction of gas and solid particles through the drag force and the associated radial flow of solid particles have been already extensively studied in the context of migration of planetisimals in protoplanetary disks. For example, Weidenschilling (1977) has noticed that in protoplanetary disks the planetesimals should migrate in the direction of increasing pressure (i.e. inward, for an axisymmetric disk with a declining radial density profile). This is due to the fact that the gas in protoplanetary disks generally orbits the central protostar at the sub-Keplerian velocity due to a substantial contribution of pressure gradients in the gas rotation curve. The cold planetesimals (which by implication have no pressure) are then forced to flow inward if the frictional orbital coupling between the gas and planetesimals is not too strong. This mechanism however may not work on galactic scales because the contribution of the pressure gradients to the gas rotation velocity may be negligible (see Sect. 2.2). In fact, the pressure gradients may even assist the gravity in some disk galaxies with a ring-like radial distribution of gas. Another interesting aspect of gas-planetesimal interaction in self-gravitating, protoplanetary disks was investigated by Rice et al. (2004). They considered disks with a flocculent spiral structure and demonstrated that the drag force rather than gravitational field of spiral arms plays a dominant role in the dynamics of planetesimals of intermediate size, forcing them to concentrate in the gas spiral arms. The non-axisymmetric gravitational field of grand-design spirals (considered in the present paper) is by implication much stronger than that of flocculent spirals. As a consequence, the trajectories of dust particles can be considerably influenced by the spiral gravitatioanl field (Fig. 5). We believe that the resonant action of spiral gravitational field on dust particles (rather than the drag force between the gas and dust) is the main driving force for the radial outward transport of dust in grand-design spiral galaxies. This conjecture is justified by the fact that the radial flow of dust takes place near the corotation resonance where a weaker frictional coupling between the dust and gas occurs (see Fig. 9).

Acknowledgements

We are grateful to Dr. Carol Jones for carefully reading the manuscript and correcting the English language usage. We are thankful to the anonymous referee for an insightful report that helped improve the final presentation. EIV gratefully acknowledges present support from a CITA National Fellowship.

Part of this work (YS) was supported by *Deutsche Forschungsgemeinschaft, DFG* (project SFB TP B3). The simulations were partly performed on the Shared Hierarchical Academic Research Computing Network (SHARCNET) cluster.

References

Bianchi, S., Alton, P. B., Davies, J. I., 2000, in: ISO Beyond Point Sources, R. J. Laureijs, K. Leech, M. F. Kessler, eds., p. 149

Binney, J., Tremaine, S. 1987, Galactic Dynamics (Princeton: Princeton Univ. Press)

Cho, J., Lazarian, A., Honein, A., Knaepen, B., Kassinos, S., Moin, P., 2003. ApJ, 589, L77

Dettmar, R.-J., Shaginyan, A. S., Shchekinov, Yu. A., 2005. A&A, submitted

Draine, B. T., Salpeter, E. E., 1979. ApJ 213, 77

Dwek, E. 1998., ApJ 501, 643

Ferrara, A., Ferrini, F., Barsella, B., Franco, J., 1991. ApJ 381, 137

Gómez, G. C., Cox, D. P., 2002. ApJ 580, 235

Howk, J.C., Savage, B.D., 1997. AJ 114, 2463

Howk, J.C., Savage, B.D., 1999. AJ 117, 2077

Kennicutt, R. C., 1981. AJ 86, 1847

Kennicutt, R. C., 1989. ApJ 344, 658

Kennicutt, R. C. 1998, ApJ, 498, 541

Köppen, J., & Arimoto, N. 1991, A&AS, 87, 109

Lin, C. C., Yuan, C., Shu, F. H., 1969. ApJ 155, 721

Lisenfeld, U., Ferrara, A., 1998, ApJ 496, 145

Mac Low, M.-M., Ferrara, A., 1999. ApJ 513, 142

Martin, C., Kennicutt, R. C., 2001. ApJ 555, 301

McKee, C. F. 1989, in IAU Symp. 135, Interstellar Dust, ed. L. J. Allamandola, A. G. G. M. Tielens (Dordrecht:Kluwer), 431

Neininger, N., Guélin, M., García-Burillo, S., Zylka, R., Wielebinski, R., 1996. A&A 310, 725

Noh, H., Vishniac, E. T., Cochran, W. D., 1991. ApJ 383, 372

Norman, C.A. Ikeuchi, S., 1989. ApJ 345, 372

Rice, W. K. M., Lodato, G., Pringle, J. E., Armitage, P. J., Bonnell, I. A., 2004, MNRAS, 355, 543

Rossa, J., Dettmar, R.-J., Walterbos, R. A. M., Norman, C. A., 2004. AJ 128, 674

Shustov, B. M., Vibe D. Z., 1995. Astron. Rept 39, 578

Silich, S., Tenorio-Tagle, G., 2001. ApJ 552, 91

Spitzer, L. 1978, Physical Processes in the Interstellar Medium, (New York: Wiley)

Stone, J., M., Norman, M. L., 1992. ApJS 80, 753

Thompson, T. W. J., Howk, J. C., Savage, B. D., 2004. AJ, 128 662

Toomre, A., 1963. ApJ 138, 385

Trewhella, M., Davies, J. I., Alton, P. B., Bianchi, S., 2000. ApJ 543, 153

Vorobyov, E. I., 2003. A&A, 407, 913

Weidenschilling, S., 1977, MNRAS, 180, 57

Weingartner, J. C., Draine, B. T., 2001. ApJ 553, 581

Xilouris, E. M., Byum, Y. I., Kylafis, W. D., Paleologou, E. V., Papamastorakis, J., 1999. A&A 344, 868

Yan, H., Lazarian, A., Draine, B. T., 2004. ApJ 616, 895

Radial transport of dust in spiral galaxies

E. I. Vorobyov [a,b], Yu. A. Shchekinov [c]

[a] *Department of Physics and Astronomy, University of Western Ontario, London, Ontario, N6A 3K7, Canada*

[b] *Institute of Physics, Stachki 194, Rostov-on-Don, Russia*

[c] *Department of Physics, Rostov State University, Rostov on Don, Russia*

Abstract

Motivated by recent observations which detect dust at large galactocentric distances in the disks of spiral galaxies, we propose a mechanism of outward radial transport of dust by spiral stellar density waves. We consider spiral galaxies in which most of dust formation is localized inside the corotation radius. We show that in the disks of such spiral galaxies, the dust grains can travel over radial distances that exceed the corotation radius by roughly 25%. A fraction of the dust grains can be trapped on kidney-shaped stable orbits between the stellar spiral arms and thus can escape the destructive effect of supernova explosions. These grains form diffuse dusty spiral arms, which stretch 4-5 kpc from the sites of active star formation. About 10% of dust by mass injected inside corotation, can be transported over radial distances $3-4$ kpc during ≈ 1.0 Gyr. This is roughly an order of magnitude more efficient than can be provided by the turbulent motions.

Key words: galaxies: spiral, ISM: dust
PACS: 98.58.Ca, 98.52.NR

1 Introduction

Interstellar dust has been recently recognized to spread over large distances from their source, and thus can be considered as a tracer of dynamical processes responsible for the circulation of material in disk galaxies. Observations of edge-on galaxies reveal a great amount of dust far outside the galactic planes: in NGC 891 and NGC 4212 dusty clouds extend up to $z \sim 2$ kpc above

Email addresses: vorobyov@astro.uwo.ca (E. I. Vorobyov), yus@phys.rsu.ru (Yu. A. Shchekinov).

the plane, and contain in total as much as $\sim 10^8\ M_\odot$ (Howk and Savage, 1997, 1999; Rossa et al., 2004, Thompson et al., 2004). Several mechanisms can contribute to transport of dust in the vertical direction: convective motions or bore flows (Gómez and Cox, 2002) associated with spiral density waves, chimneys produced by multiple supernova explosions (Norman and Ikeuchi, 1989), and radiation pressure (Ferrara et al., 1991; Shustov and Vibe, 1995; Dettmar et al., 2005).

The situation is less clear when the radial distribution of dust is considered. Observations of spiral galaxies in the far infrared band show that dust can extend in the radial direction far beyond the stellar disks. Neininger et al. (1996) found that the radial distribution of 1.2 mm dust emission from NGC 4565 is two times wider than CO emission. ISO observations of several spiral galaxies at 200 μm (Trewhella et al., 2000; Bianchi et al., 2000) revealed the presence of relatively cold dust outside the stellar disks with a scale length $R_d \gtrsim 1.5\ R_*$ (R_d and R_* are the radial scales of dust and stars, respectively). A similar conclusion was made by Xilouris et al. (1999) for four spirals observed in the optical and near infrared bands. Bianchi et al. (2000) found that the best fit of the 200 μm emission for NGC 6946 gives $R_d \gtrsim 3\ R_*$. MHD turbulence can, in principle, spread dust outward in radial direction (Cho et al., 2003), however, the corresponding time for galactic scales seems to be too long. Indeed, the coefficient of turbulent diffusion $D \sim \langle Lv \rangle / 3$ is of the order of 10^{26} cm^2 s^{-1} for typical interstellar values $L \sim 100$ pc and $v \sim 10$ km s^{-1}. Therefore, dust particles can diffuse by turbulent motions over scales $\sqrt{\langle \Delta R^2 \rangle} > 3$ kpc in a characteristic time $t > 16$ Gyr. In these conditions, only regular hydrodynamic motions can explain the presence of dust outside stellar disks in spiral galaxies.

In this paper we explore the possibility that the radial transport of dust in spiral galaxies is driven by the hydrodynamic motions associated with spiral stellar density waves. In Sect. 2 a set of model hydrodynamic equations for dusty interstellar medium is described and the equilibrium parameters are fixed. In Sect. 3 the generation of spiral pattern in the stellar disk is formulated. Sect. 4 describes trajectories of single dust particles and Sect. 5 describes the dynamics of dust fluid as a whole including formation of dusty spiral arms. Sect. 6 summarizes our results.

2 Model description

2.1 Basic equations

Our model disk is a two-fluid system composed of dust and gas, which evolves in the external potential of the stellar disk and dark matter halo. We assume that the dust and gas are coupled by friction. The gas disk is isothermal at $T = 10^4$ K and the dust pressure is negligible. We use the thin disk approximation, i.e. all quantities are vertically integrated. The system is described by the basic hydrodynamic equations, where we denote the dust and gas by the subscripts d and g, respectively.

The continuity equation for the gas and dust is

$$\frac{\partial \Sigma_{\rm g,d}}{\partial t} + \boldsymbol{\nabla} \cdot (\Sigma_{\rm g,d}\, \boldsymbol{v}_{\rm g,d}) = 0, \tag{1}$$

where $\Sigma_{\rm g,d}$ are the gas and dust surface densities and $\boldsymbol{v}_{\rm d,g}$ are their velocities.

The equations of motion are

$$\frac{\partial \boldsymbol{v}_{\rm g}}{\partial t} + (\boldsymbol{v}_{\rm g} \cdot \boldsymbol{\nabla})\boldsymbol{v}_{\rm g} = -\boldsymbol{\nabla}\Phi_{\rm s1,s2,h} - \frac{\boldsymbol{\nabla} P_{\rm g}}{\Sigma_{\rm g}} + \frac{\Sigma_{\rm d}\boldsymbol{f}}{\Sigma_{\rm g}}, \tag{2}$$

$$\frac{\partial \boldsymbol{v}_{\rm d}}{\partial t} + (\boldsymbol{v}_{\rm d} \cdot \boldsymbol{\nabla})\boldsymbol{v}_{\rm d} = -\boldsymbol{\nabla}\Phi_{\rm s1,s2,h} - \boldsymbol{f}, \tag{3}$$

where, $\Phi_{\rm s1}, \Phi_{\rm s2}$, and $\Phi_{\rm h}$ are the contributions to the total gravitational potential by the axisymmetric stellar disk, non-axisymmetric spiral density perturbation, and dark matter halo, respectively. The friction force is defined as $\boldsymbol{f} = A(\boldsymbol{v}_{\rm d} - \boldsymbol{v}_{\rm g})$ (see Draine and Salpeter, 1977; Noh et al., 1991).

We take the friction coefficient A to be a simple function of the disk conditions. We assume that the thickness of the dust disk is comparable to that of the gas disk. Then the collisional timescale $\tau_{\rm c}$ of energy and momentum exchange between the gas and dust particles may be used as an estimate of A^{-1},

$$A \sim \tau_{\rm c}^{-1} = \frac{\sigma_{\rm c} n_{\rm g} v_{\rm th} m_{\rm g}}{m_{\rm d}}, \tag{4}$$

where $n_{\rm g}$ is the number density of gas particles, $m_{\rm g}$ and $m_{\rm d}$ are the masses of gas and dust particles, and $v_{\rm th} = \sqrt{3RT/\mu}$ is the gas velocity dispersion; $\tau_{\rm c}$ is estimated for the subsonic relative motion of neutral dust grains and gas. Since we use the thin disk approximation, the gas volume density in Eq. (4) is approximated assuming a local vertical hydrostatic equilibrium $m_{\rm g} n_{\rm g} = \Sigma_{\rm g}/z_0$,

where the gas disk thickness is defined as[1] $z_0 = 2c_s^2/(\pi G\Sigma_{\rm g})$, where $c_{\rm s}$ is the sound speed. The geometrical cross section is used as an estimate of the collisional cross section $\sigma_{\rm c} = \pi a^2$, where a is the average radius of a dust particle. In the present simulations, we assume $m_{\rm d} = 10^{-14}$ g and $a = 10^{-5}$ cm. It is well known that interstellar dust grains are charged, and Coulomb interactions with charged ambient ions and electrons increase the friction force (Draine and Salpeter, 1979; Weingartner and Draine, 2001). However, as we are mostly concerned with the diffuse HI phase of the ISM (warm neutral medium, WNM, in standard nomenclature), this increase does not crucially change the resulting friction coefficient. Indeed, the Coulomb friction can be written as $F_{\rm C} = \chi(Z)F^0_{\rm HI}$, where $F^0_{\rm HI}$ is the friction in an HI environment, $\chi(Z) = \langle a_Z/a\rangle^2 \ln\Lambda \sum\limits_i x_i(m_i/m_p)$, $a_Z = Ze^2/kT$, $\ln\Lambda$ is the Coulomb logarithm, x_i is the fractional ionization of i-th ions or electrons, m_i is the corresponding mass, averaging is over charge distribution of dust grains (Weingartner and Draine, 2001). For typical conditions in the WNM; $x \sim 0.1$, $n \sim 0.3$ cm^{-3}, and dust charge $\langle Z\rangle \simeq 60$ (Yan et al., 2004) we get $\chi \sim 1$. Therefore, we will restrict our consideration with the friction coefficient A as determined for the neutral dust.

2.2 Equilibrium gas disk

Initially, our model galaxy consists of a rotating gas disk balanced by the gravity of an *axially symmetric* stellar disk and spherically symmetric dark matter (DM) halo. The dust disk is introduced later when the non-axisymmetric part of the stellar gravitational potential is set. The rigid stellar disk is assumed to have a power-law radial density profile of the form

$$\Sigma_{\rm s}(r) = \frac{B^2}{2\pi G}\left[(r_{\rm s}^2 + r^2)^{-3/2}\right], \tag{5}$$

where $B^2 = 2\pi G r_{\rm s}^3 \Sigma_{\rm s0}$. The gravity force of such a density distribution is given by Toomre (1963)

$$\frac{\partial \Phi_{\rm s1}}{\partial r} = B^2\left[\frac{r}{r_{\rm s}}(r_{\rm s}^2 + r^2)^{-3/2}\right]. \tag{6}$$

In the following, we use the central stellar density $\Sigma_{\rm s0} = 1.2 \times 10^3\ M_\odot$ pc^{-2} and $r_{\rm s} = 3$ kpc, which gives us a total stellar mass of $M_{\rm st} = 7 \times 10^{10}\ M_\odot$.

[1] Since the dominant component of gravity in the vertical direction is the stellar disk, the total surface density ($\Sigma_{\rm tot} = \Sigma_{\rm g} + \Sigma_{\rm s}$) should appear in the expression for z_0. This may increase the friction coefficient A, especially in the inner regions. We discuss this issue in Sect. 5

The density distribution of the rigid DM halo is assumed to be that of a modified isothermal sphere (Binney and Tremaine, 1987)

$$\rho_{\rm h} = \frac{\rho_{\rm h0}}{(1 + r/r_{\rm h})^2}, \tag{7}$$

where the central density $\rho_{\rm h0}$ and the characteristic scale length $r_{\rm h}$ are given by Mac Low and Ferrara (1999) and Silich and Tenorio-Tagle (2001):

$$\rho_{\rm h0} = 6.3 \times 10^{10} \left(\frac{M_{\rm h}}{M_\odot}\right)^{-1/3} \; h^{-1/3} \; M_\odot \; {\rm kpc}^{-3} \tag{8}$$

$$r_{\rm h} = 0.89 \times 10^{-5} \left(\frac{M_{\rm h}}{M_\odot}\right)^{1/2} \; h^{1/2} \; {\rm kpc}. \tag{9}$$

Here, h is the Hubble constant in units of 100 km s^{-1} Mpc^{-1} and $M_{\rm h} = 10^{12}\ M_\odot$ is the total DM halo mass. We note that the DM halo mass within the computational domain $r < 20$ kpc is $M_{\rm h}(r < 20\ {\rm kpc}) = 5 \times 10^{10}\ M_\odot$. We adopt $h = 0.65$ throughout the paper. The gravitational force of spherically symmetric DM halo can be expressed as

$$\frac{\partial \Phi_{\rm h}}{\partial r} = 4\pi G \rho_{\rm h0} r_{\rm h} \left[r/r_{\rm h} - \arctan(r/r_{\rm h})\right] \left(\frac{r_{\rm h}}{r}\right)^2. \tag{10}$$

The gas disk has an exponentially declining density profile with the central surface density $\Sigma_{\rm g0} = 30\ M_\odot$ pc^{-2}, and radial scale length $r_{\rm g} = 9$ kpc. The total mass of the gas disk within the computational domain ($r = 20$ kpc) is $M_{\rm g} = 1.0 \times 10^{10}\ M_\odot$. The gas disk contains only a small fraction ($\sim 10\%$) of the total mass in the computational domain. Hence to a first approximation we can assume that the gas moves in the potential field of the stars and DM halo.

Once the density profile of the gas disk is fixed, its initial rotation curve (RC) is obtained by solving Eq. (2), where the friction force f is set to zero and the time variations are neglected. The resulting initial RC is plotted in Fig. 1, where it reaches a maximum circular velocity of 200 km s^{-1} at $r \approx 3$ kpc. Beyond this maximum, the rotational velocity undergoes a gradual decline. Because the gas surface density has a slowly declining radial profile ($r_{\rm g} = 9$ kpc) and the gas is assumed to be isothermal, the contribution of the pressure gradient in the gas rotation curve is less than 1% everywhere in the disk.

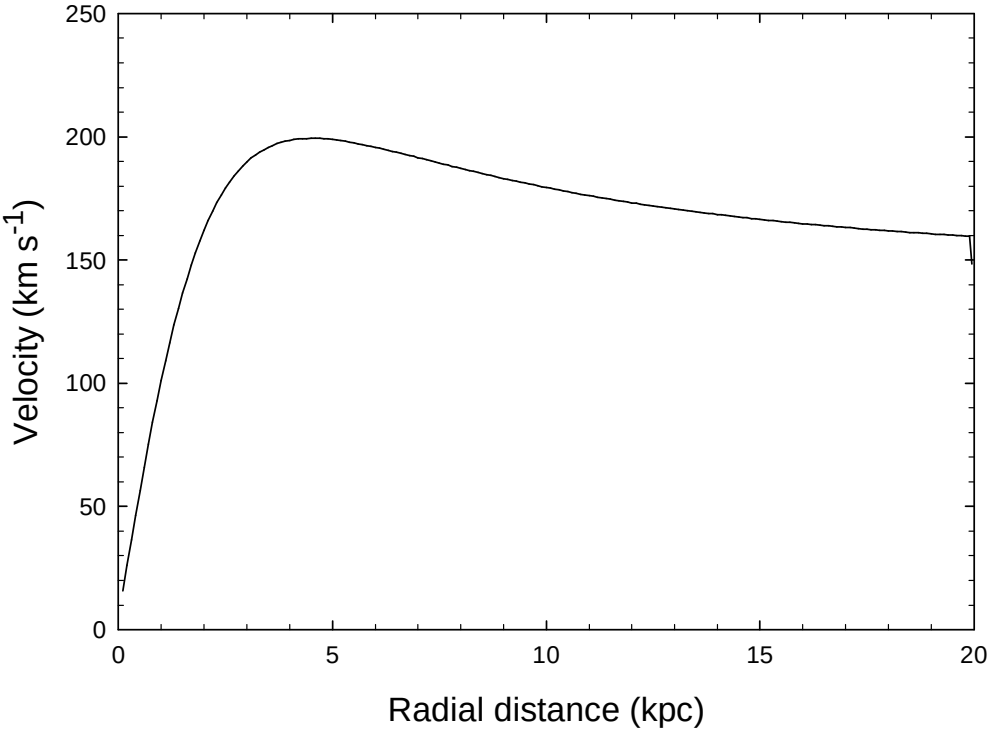

Fig. 1. The initial rotation curve of the gas disk.

2.3 Computational techniques

A set of hydrodynamic equations (1)-(3) in polar coordinates (r, ϕ) is solved using the method of finite-differencing with a time-explicit, operator-split solution procedure (ZEUS-2D) described in detail in Stone and Norman (1992). We use a resolution of 200×200 grid points in a polar computational domain with a radius of 20 kpc. We set a free boundary condition at the outer boundary, i.e. the gas and dust are allowed to flow out freely from the computational domain. The outflowing gas/dust is assumed to be lost by the parent galaxy.

3 Generation of spiral pattern

Once the axisymmetric equilibrium gas disk is constructed, we introduce the non-axisymmetric spiral gravitational potential of the stellar disk Φ_{s2}. The latter is defined in the form of a running spiral density wave (Lin et al., 1969)

$$\Phi_{s2} = -C(r) \cos\left[m(\cot(i) \ln(r/r_{sp}) + \phi - \Omega_{sp} t)\right]. \quad (11)$$

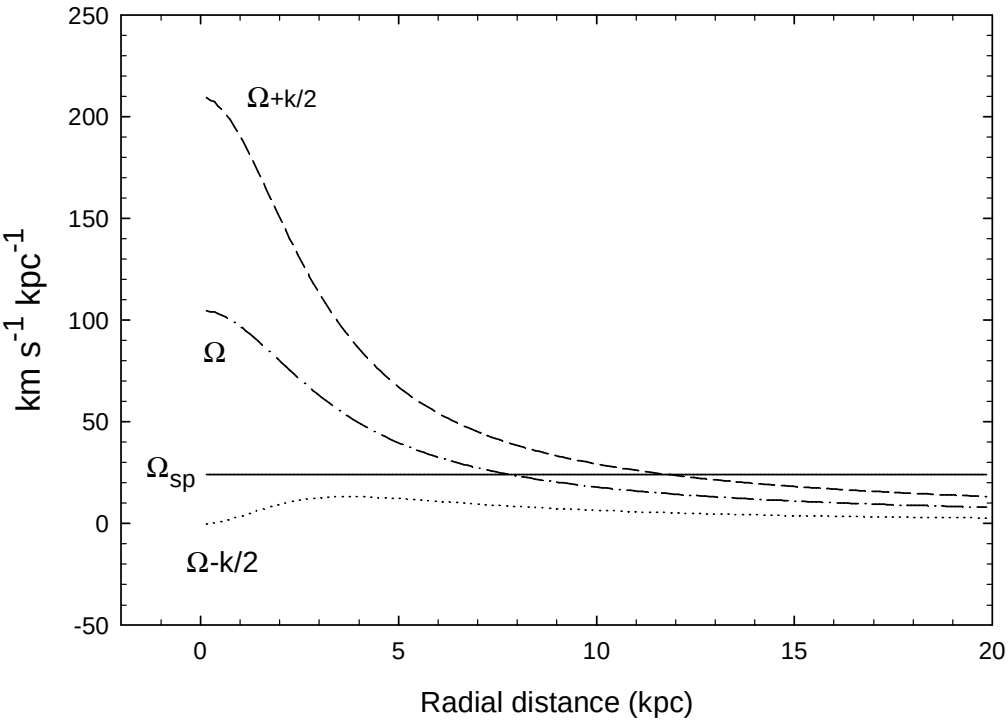

Fig. 2. Behaviour of $\Omega \pm \kappa/2$, where κ is the epicyclic frequency and Ω is the angular velocity of gas. The angular velocity of spiral pattern $\Omega_{\rm sp}$ is shown by the solid line.

Here, $C(r)$ is the amplitude of the spiral gravitational potential, m is the number of spiral arms, i is the pitch angle, $r_{\rm sp}$ is the characteristic winding length of spiral arms, and $\Omega_{\rm sp}$ is the angular velocity of spiral pattern. In the following we adopt $m = 2$, $i = 25^\circ$, $r_{\rm sp} = 6$ kpc, $\Omega_{\rm sp} = 24$ km s^{-1} kpc^{-1}. This choice of $\Omega_{\rm sp}$ places the corotation of the gas disk at ≈ 8.0 kpc and the outer Lindblad resonance at ≈ 12.0 kpc. The inner Lindblad resonance is absent. The behavior of gas angular velocity Ω and $\Omega \pm \kappa/2$ is shown in Fig. 2. According to Kennicutt (1981), a pitch angle of $i = 25^\circ$ is typical for Sc galaxies. The efficiency of radial transport of dust for different pitch angles is discussed in Sect. 5.

The logarithmic spiral defined by Eq. (11) is quickly winding up as $r \to 0$. This may create large gradients of gravitational potential near the origin and lead to serious numerical difficulties. For instance, if the amplitude $C(r)$ is independent of r, than the ratio of maximum non-axisymmetric perturbing force to the total axisymmetric gravity force $\beta(r) = max|\nabla\Phi_{\rm s2}|/(\partial\Phi_{\rm s1}/\partial r + \partial\Phi_{\rm h}/\partial r)$ sharply increases as $r \to 0$. This is illustrated in Fig. 3, where $\beta(r)$ is plotted by the dotted line for $C = 0.005$ (in dimensionless units). The apparent growth of β with radius for $r > 3$ kpc is also unrealistic since the spiral arms are expected to vanish at larger radii. In view of these difficulties, we use a radially dependent amplitude of the form $C(r) = C_0(r)^{\alpha(r)}$. Here,

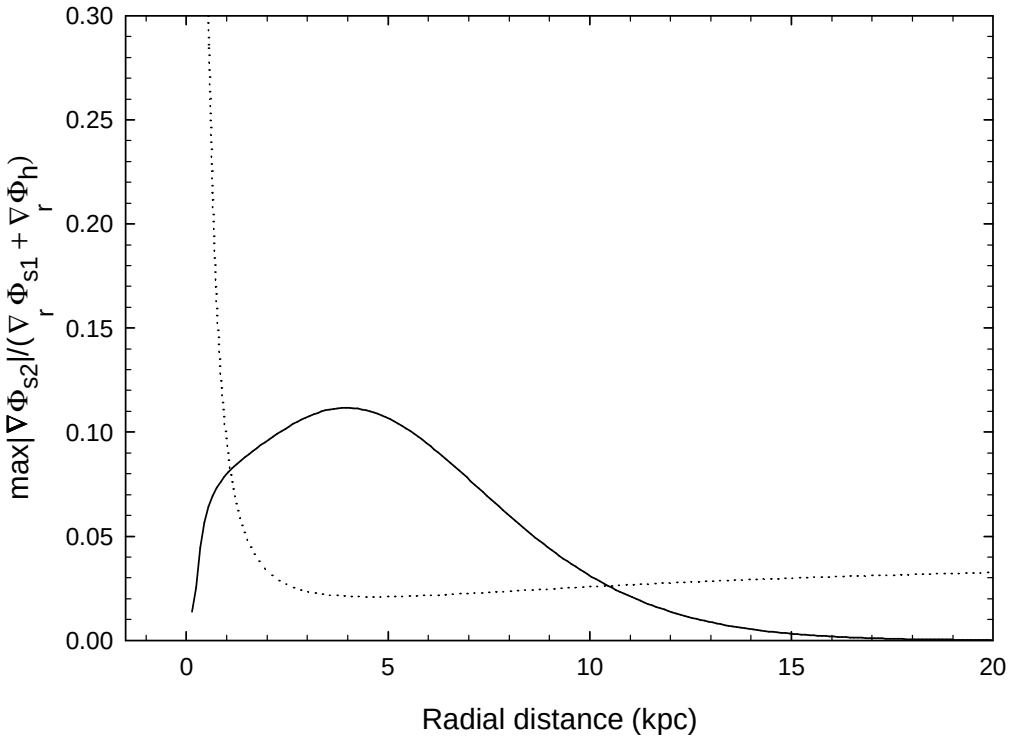

Fig. 3. The ratio of the maximum, non-axisymmetric perturbing force $|\boldsymbol{\nabla}\Phi_{\rm s2}| = [(\partial\Phi_{\rm s2}/\partial r)^2 + (r^{-1}\partial\Phi_{\rm s2}/\partial\phi)^2]^{1/2}$ to the total axisymmetric gravity force $(\partial\Phi_{\rm s1}/\partial r + \partial\Phi_{\rm h}/\partial r)$ as a function of radial distance. The solid and dashed lines are explained in greater detail in the text.

$C_0(r)$ is a linear function of r which has a value of 0 at $r = 0$ kpc (ensuring that $|\boldsymbol{\nabla}\Phi_{\rm s2}|$ diminishes as $r \rightarrow 0$) and attains its maximum value of 0.0045 (in dimensionless units) at $r = 20$ kpc. The exponent $\alpha(r)$ decreases linearly with radius from $\alpha = 2$ at r=0 kpc to $\alpha = -2.1$ at r=20 kpc. The resulting profile of $\beta(r)$ is shown in Fig. 3 by the solid line. Since the non-axisymmetric gravity force scales as $|\boldsymbol{\nabla}\Phi_{\rm s2}| \propto 1/r^{1-\alpha(r)}$, the ratio β increases with radius at $r < 4$ kpc, and decreases at $r \gtrsim 4$ kpc. At the position of corotation $r_{\rm cr} \approx 8$ kpc, β drops by roughly a factor of 2 as compared to its maximum value at $r \approx 4$ kpc and continues to decrease at larger radii. We note that the maximum, non-axisymmetric perturbing force never exceeds 12% of the total axisymmetric gravity force.

The non-axisymmetric part of the stellar gravitational potential $\Phi_{\rm s2}$ is turned on slowly. Specifically, $\Phi_{\rm s2}$ is multiplied by a function $\epsilon(t)$, which has a value of 0 at t=0 and linearly grows to its maximum value of 1.0 at $t \geq 200$ Myr. It takes a few hundred Myr for the gas disk to adjust to the spiral distortion and develop a spiral structure as shown in Fig. 4. The gas spiral pattern (as well as the stellar one) rotates counterclockwise. The position of corotation

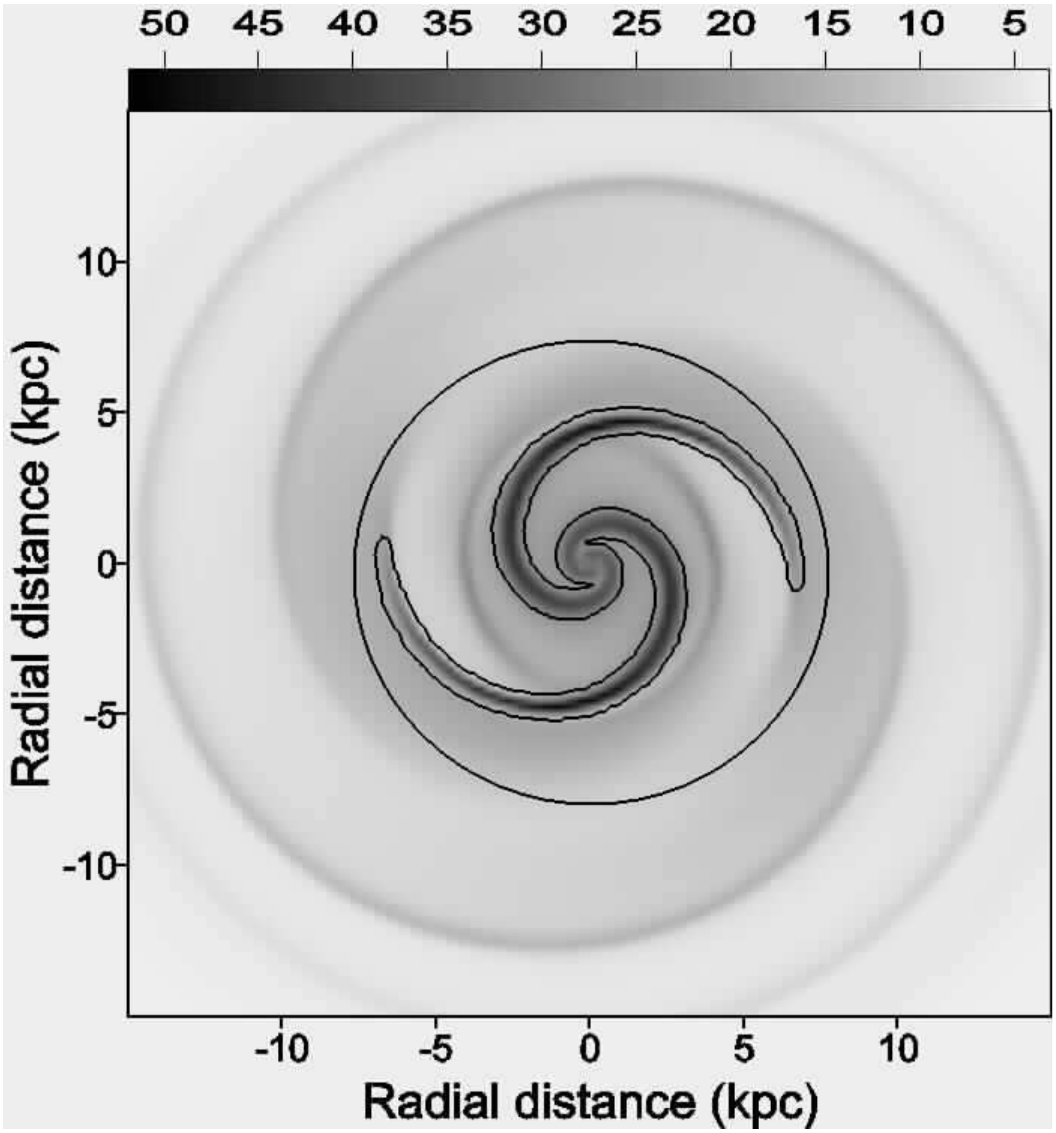

Fig. 4. Gas density distribution at $t = 0.8$ Gyr from the beginning of numerical simulations. The corotation radius is shown by the circle. The scale bar is in $M_\odot$ pc^{-2}. The contour line sketches the region of supercritical gas density (see Sect. 5 for details).

is shown by the circle. The strongest gas response to the underlying stellar spiral density wave is seen inside the corotation circle. However, a weak spiral structure can still be traced outside corotation at radii $r = 10 - 15$ kpc.

4 Trajectories of dust particles

In this section we study the trajectories of single dust particles in the combined gravitational potential of stellar disk and dark matter halo including

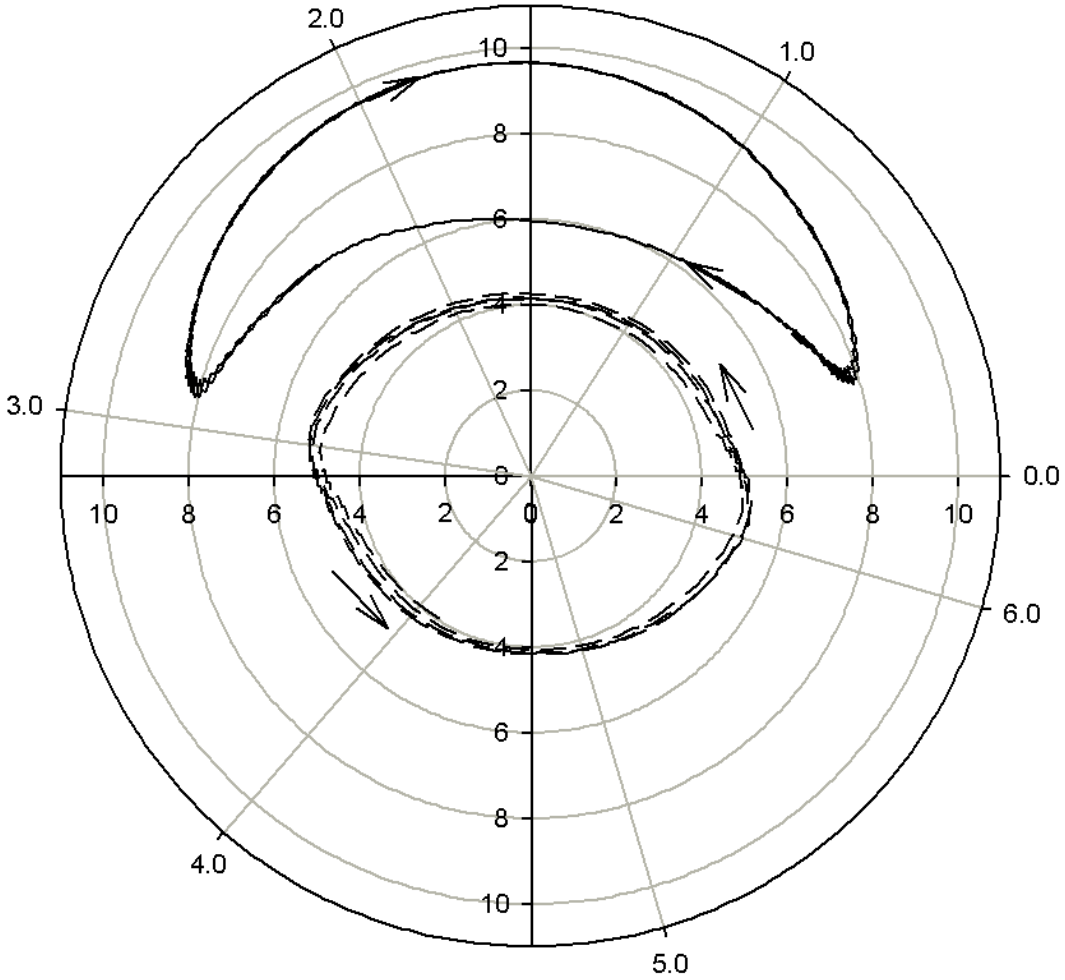

Fig. 5. Polar plot (r, θ) showing trajectories of three test dust particles. The radial distance is in kiloparsecs and the azimuthal angle is in radians. Stellar spiral arms are located along azimuthal angles of 0 and π. The direction of motion of test particles in the frame of reference of stellar spiral arms is indicated by arrows.

the effects of dust-gas friction. The equation of motion of the dust fluid (3) can be obviously reduced to a set of equations of motion for a single dust particle and subsequently solved using the Runge-Kutta scheme. We introduce test dust particles at different radial distances from the galactic centre $r_{\rm d}$ and at different azimuthal angles $\theta_{\rm d}$ with respect to the position of stellar spiral arms. In our simulations, the stellar spiral arms are modeled by the spiral gravitational potential rotating counterclockwise in the laboratory frame of reference. Therefore, the position of stellar spiral arms at any given time is determined as the position of minimum in the spiral gravitational potential defined by Eq. (11). All dust particles are injected at $t = 0.8$ Gyr when the gas spiral structure is fully developed (see Fig. 4), and they are assigned velocities drawn from the parent gas. We followed the trajectories of test dust particles for 2 Gyr.

The phase $(r_{\rm d}, \theta_{\rm d})$ trajectories of three representative dust particles *in the*

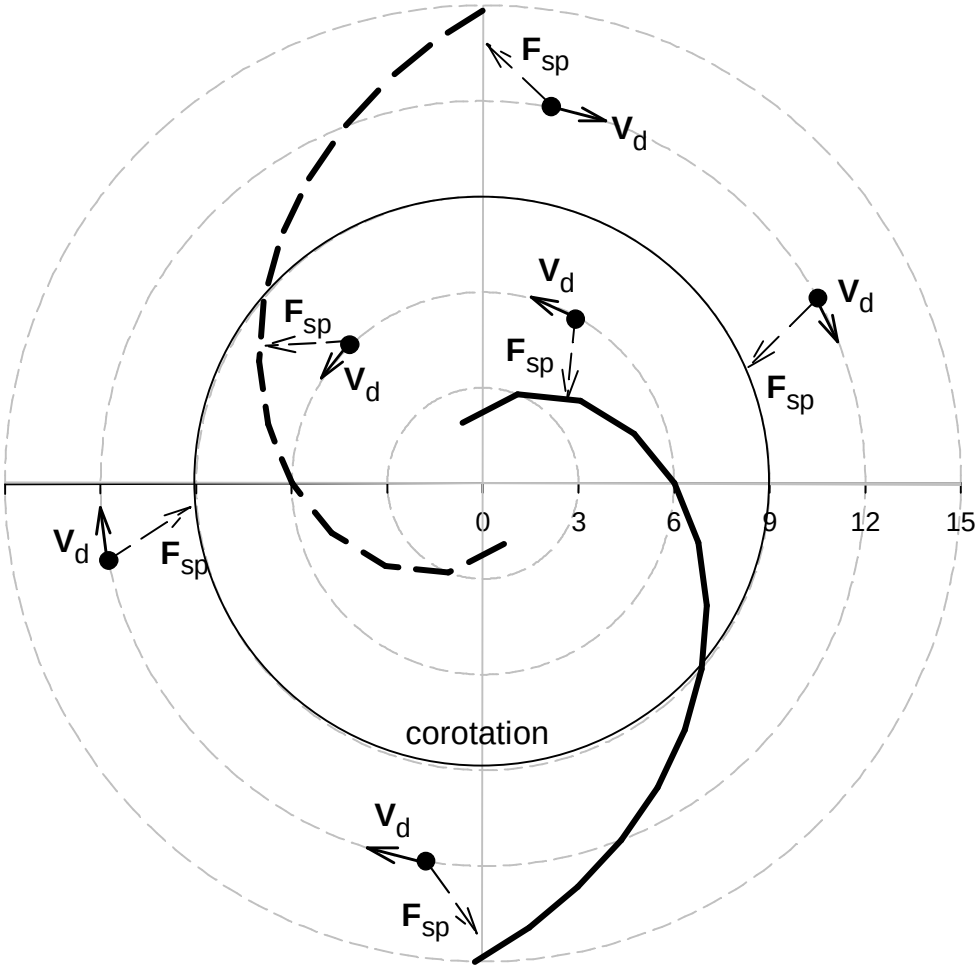

Fig. 6. Schematic description of gravity forces (shown by the dashed arrows) acting on test dust particles from the stellar spiral arms (plotted by thick solid and dashed lines). Velocities of dust particles in the frame of reference of stellar spiral arms are indicated by solid arrows. Two test particles inside corotation and four test particles outside corotation are shown. Arrows are not to scale.

frame of reference of stellar spiral arms are shown in Fig. 5. The stellar spiral arms in Fig. 5 are always located along azimuthal angles $\theta_{\rm sp} = 0$ and π. The dashed line shows the trajectory of a dust particle placed initially at $r_{\rm d}$=5.0 kpc in the arm ($\theta_{\rm d} = 0$; hereafter, particle 1), whereas the solid line gives the trajectory of a dust particle placed initially at $r_{\rm d}$=7.0 kpc in the interarm region ($\theta_{\rm d} = \pi/4$; hereafter, particle 2). Dust particles similar to particle 1 may be injected by supernova explosions which tend to occur near spiral arms. Particle 2 may be created by red giant stars.

It is apparent that the trajectories of particles 1 and 2 are quite different. Particle 1 moves on an elliptical orbit in one direction (counterclockwise), remaining always inside the corotation circle ($r_{\rm cr} \approx 8.0$ kpc). The trajectory

of particle 1 is fairly stable. It comes closer to the origin when traveling between the arms ($\theta_{\rm d} \approx \pi/2$) and it passes through the spiral arms 4 times during 0.65 Gyr. Since dust particles are thought to be destroyed by supernova explosions, such a frequent encounter with the spiral arms implies that particle 1 may not live longer than 0.5 Gyr (although it depends on the covering factor of sufficiently strong shock waves, $v_{\rm SN} \gtrsim 100$ km s^{-1}, generated by supernova explosions (SNe) and propagating perpendicular to the spiral arms). Particle 2 has a stable, kidney-shaped trajectory, which shows an impressive radial migration of ~ 4 kpc, as opposed to only 1 kpc for particle 1. Interestingly, particle 2 is caught between the spiral arms, periodically passing through the corotation circle from the inner part of the disk to the outer part and vice versa. Since particle 2 never encounters the spiral arms during 2 Gyr, it may live significantly longer than particle 1. Dust particles that are born at $\theta_{\rm d} \approx \pi/2$ (i.e. exactly between the spiral arms) but are sufficiently away from the galactic center, move on much more compact orbits as shown by the dotted line in Fig. 5.

To summarize, we find that all particles born at $r < 6$ kpc, i.e. $\gtrsim 2.0$ kpc away from the position of corotation radius $r_{\rm cr} \approx 8.0$ kpc, always stay inside corotation. This is irrespective of their azimuthal angles of birth. Trajectories of those dust particles resemble that of particle 1 shown in Fig. 5 by the dashed line. Such particles often encounter spiral arms and thus may be destroyed in one rotation period by shocks from SNe. The fraction of surviving dust grains is determined by the probability for them to meet a sufficiently strong ($v_s \gtrsim 100$ km s^{-1}) destroying shock wave inside the arm. On the other hand, particles injected near corotation at 6 kpc $\lesssim r < 8.0$ kpc (and sufficiently away from spiral arms) spend most of their lifetime in the interarm region. Therefore, most of these dust particles can survive over the entire migration period in the outer galactic regions.

In the absence of spiral arms, dust particles move on circular orbits determined by the axisymmetric global gravitational potential of a galaxy and the drag force from the gas disk. When the non-axisymmetric spiral gravitational potential is introduced, dust particles move on various non-circular orbits as shown in Fig. 5. In order to understand the origin of such non-circular orbits, we consider the influence of a non-axisymmetric spiral gravity force on the motion of dust particles. The gravity force of spiral arms acting on moving particles is schematically plotted in Fig. 6 by the dashed arrows. Six particles are presented; two particles inside the corotation circle and four particles outside the corotation circle. The direction of motion of dust particles *in the frame of reference of the spiral pattern* is shown by the solid arrows. Two spiral arms are schematically shown by the solid and dashed lines. A moving dust particle may see the nearest spiral arm as either convex or concave. If the dust particle is closer to the concave spiral, the latter acts to increase (on average) the radial distance of the particle due to its gravitational drag.

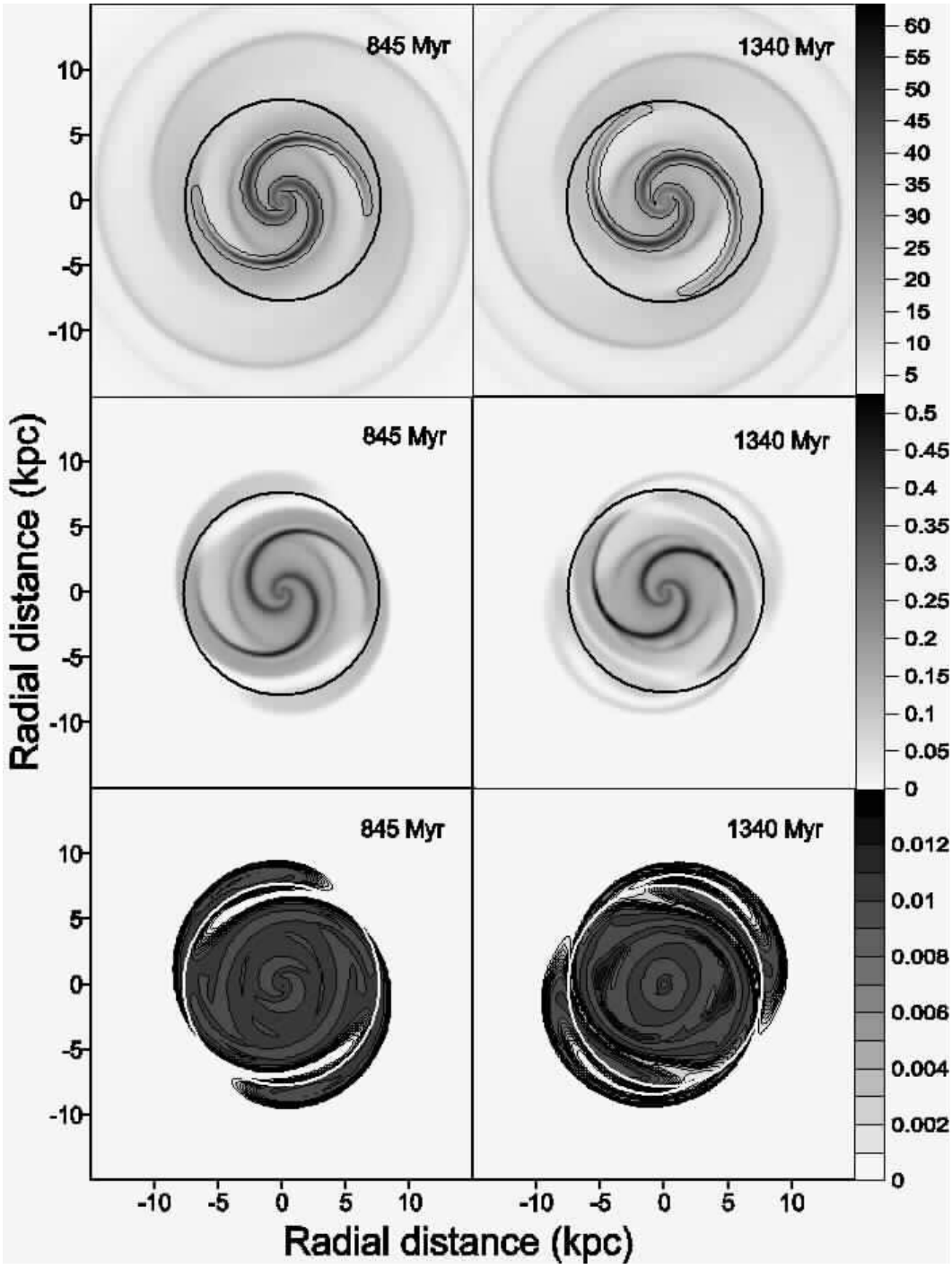

Fig. 7. Gray-scale images of the gas distribution (the upper panels), dust distribution (the middle panels) and the dust-to-gas ratio (lower panels). The elapsed time is indicated in each panel. The position of corotation of the gas disk is outlined by the circle. The scale bars in the upper and middle panels give the column density in $M_\odot$ pc^{-2}

On the contrary, if the dust particle is closer to the convex spiral, the latter tends to decrease the radial distance of the particle. If we now recall that the trailing spiral arms in Fig. 5 are located along the azimuthal angles 0 and π and rotate counterclockwise, then the effect of gravitational drag from the spiral arms becomes clearly evident in the trajectories of dust particles. For instance, when dust particles are in the first quadrant, they are attracted by the convex spiral located at $\theta_{\rm sp} = 0$. As a consequence, the radial position of these particles decreases. When dust particles enter the second quadrant, their motion is controlled by the concave spiral located at $\theta_{\rm sp} = \pi$ and their radial position increases. Therefore, the trajectories of dust grains may be sensitive to the pitch angle of stellar spiral arms. The maximum radial migrations of dust grains are expected for a pitch angle of 45°.

The action of the friction force is more difficult to assess. The friction between dust and gas may help reverse the direction of motion of a dust particle (with respect to the spiral arms) when it passes through corotation. Indeed, when the dust particle is inside the corotation circle, its velocity is larger than that of spiral arms (the same is true for the gas in general). After passing through corotation, the dust particle enters the region which is characterized by a smaller velocity than that of spiral arms. Therefore, we may expect that the friction between gas and dust would act to equalize the velocities of dust and gas, and thus decelerate the dust particles. This would eventually reverse their direction of motion with respect to the spiral arms as seen in Fig. 5 for particle 2.

5 Response of dust to the stellar spiral density wave

In this section we study how dust responds to the imposed spiral disturbance. The dominant sources of dust formation in disk galaxies are stellar winds from late-type giant and supergiant stars, supernova explosions, and growth of pre-existing grains in dense $n \gtrsim 10^3$ cm^{-3} molecular clouds (Dwek, 1998). All of these sources are mainly located inside the corotation circle. Indeed, the strongest gas response to the stellar spiral density wave in Fig. 4 is obviously seen inside corotation. We compute the critical density for star formation as defined by the Toomre criterion (Kennicutt, 1989)

$$\Sigma_{\rm crit}^{\rm Toomre} = \frac{0.7\, c_{\rm s}\, \kappa}{\pi\, G}, \qquad (12)$$

where κ is the epicyclic frequency, and the shear criterion (Martin and Kennicutt, 2001)

$$\Sigma_{\rm crit}^{\rm shear} = \frac{2.5 A_{\rm sh}\, v_{\rm s}}{\pi G}, \tag{13}$$

where $A_{\rm sh} = -0.5\, r\, {\rm d}\Omega/{\rm d}r$ is the local shear rate (the Oort constant). The contour line in Fig. 4 traces the region of supercritical density with $\Sigma_{\rm g} > \min(\Sigma_{\rm crit}^{\rm Toomre}, \Sigma_{\rm crit}^{\rm shear})$ which is evidently localized inside corotation. Although the gas density outside corotation may occasionally become supercritical (not shown in Fig. 4) especially along the outer diffuse gas spirals, a lower gas density and higher temperature as compared to the inner region can work against star formation in that region. We thus conclude that most of star formation in our model galaxy is localized within the corotation circle. The radial scale length of our old stellar disk is $r_{\rm s} = 3$ kpc which also implies that most of low to intermediate mass stars that are capable of producing dust are confined within the corotation circle.

We instantaneously inject $3.4 \times 10^7\ M_\odot$ of dust mass inside the corotation circle ($r < 7.8$ kpc) and then determine the fraction of dust that can move outside corotation. In the present simulations, the dust particles are injected at $t = 0$ Myr when a spiral structure in the gas disk has not yet developed. We also tried to introduce dust at t=800 Myr (when the gas spirals are fully developed) and confirmed that the time of dust injection has little influence on dust dynamics. The spatial distribution of injected dust is such that the dust-to-gas ratio $\gamma = 0.01$ inside corotation, and $\gamma = 0$ outside corotation. The velocity of injected dust is equal to that of the gas. A conservative estimate of dust-to-gas mass ratio in the solar neighborhood gives an average value of $\gamma = 0.006$ ranging from 0.002 up to 0.04 in H_2 regions (Spitzer, 1978).

The upper and middle panels in Fig. 7 show two snapshots of the evolution of the gas and dust surface densities, respectively, whereas the lower panels give the dust-to-gas mass ratio. The numbers in each panel indicate the elapsed time since the beginning of the simulation. The circle indicates the position of corotation of the gas disk. A strong spiral response to the stellar density wave develops in the dust disk after approximately 3 revolution periods of our model galaxy. The dust density closely follows that of gas in the inner regions of our model galaxy. Small radial and azimuthal variations of the dust-to-gas ratio around the initial value 0.01 are indicative of a dominant role of frictional force in the dynamics of dust in the inner 5 kpc. This is in agreement with the results of Sect. 4 where we have found that dust particles born in the inner 5 kpc move on fairly stable elliptical orbits around the galactic center. At larger radii 6 kpc $\lesssim r < 8.0$ kpc, however, significant variations of γ become evident. There are regions near corotation that are completely devoid of dust, even though the initial dust-to-gas ratio is 0.01. A noticeable portion of dust is

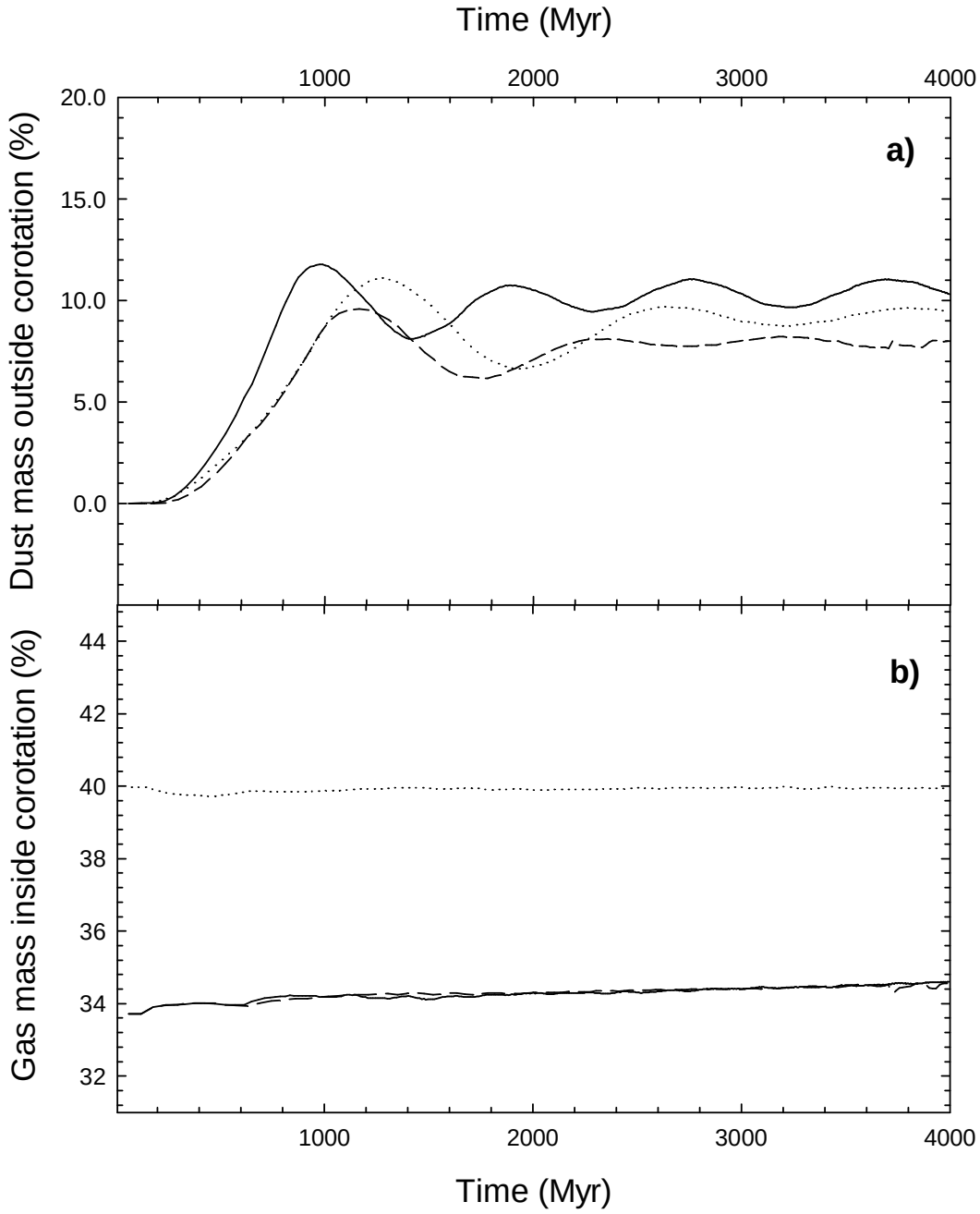

Fig. 8. **a)** Dust mass ouside corotation as a percentage of the total dust mass. The solid and dashed lines correspond to the models with pitch angles of stellar spiral density wave $i = 25^\circ$ and $i = 15^\circ$, respectively. The dotted line gives the dust mass outside corotation for a lower rotation frequency of stellar spirals $\Omega_{\rm sp} = 21$ km s^{-1} kpc^{-1}. **b)** Gas mass inside corotation as a percentage of the initial total gas mass. The solid, dashed, and dotted lines correspond to the same models as in the upper panel. The difference in the values of the gas fraction inside corotation for $\Omega_{\rm sp} = 21$ km s^{-1} kpc^{-1} and $\Omega_{\rm sp} = 24$ km s^{-1} kpc^{-1} is due to the different positions of the corotation radius in the two cases.

observed outside corotation. This dust tends to form into diffuse outer spiral arms, which appear to be a smooth extension of the inner dust spiral arms and can be traced up to $r = 10$ kpc. The dust-to-gas ratio in the outer dust arms is not dissimilar to that of the inner $r < 5$ kpc region. We thus conclude that the perturbing force of stellar spirals starts to play an important role in the dust dynamics near corotation resulting in an outward radial transport of dust. If we now identify the regions of supercritical gas density by contour lines in the upper panels of Fig. 7, than it becomes evident that the dust component can be found as far as 4-5 kpc from the sites of active star formation.

The solid line in Fig. 8a gives the dust mass outside corotation (as a percentage of the total dust mass) versus time elapsed since the injection of dust. Approximately 10% of the initial injected dust mass is transported outside corotation during 1 Gyr. This implies that the dust transport rate is $\dot{M} = 3.8\ M_{\odot}\ \mathrm{Myr}^{-1}$. At later times, the amount of transported dust varies around $\approx 10\%$ of the total dust mass. These variations are mainly due to dust particles born inside the corotation circle in the interarm region, where they are trapped into periodic orbits as shown by solid and dotted lines in Fig.5. We conclude that only a (small) fraction of dust particles (approximately 10% by mass) injected instantaneously inside the corotation circle can move to the outer regions, while the rest is confined in the inner galaxy. As a consequence, the radial transport of an instantaneously injected portion of dust terminates after ≈ 1 Gyr.

The spiral stellar density wave considered so far has a pitch angle of $i = 25^{\circ}$. This is typical for Sc galaxies (Kennicutt, 1981). The efficiency of outward radial transport of dust may depend on the openness of stellar spiral arms. To test this conjecture, we explored a series of models with different pitch angles. The dashed line in Fig. 8 shows the the dust mass outside corotation as a percentage of the total dust mass for the stellar spiral with a pitch angle $i = 15^{\circ}$. Roughly 8% of the injected dust mass is pushed outside corotation, as compared to $\approx 10\%$ for $i = 25^{\circ}$. This indicates that the efficiency of outward radial transport of dust drops by roughly 2%. We expect that the radial transport of dust by spiral stellar density waves may becomes inefficient for very tightly wound spirals with a pitch angle $i \lesssim 5^{\circ}$. Our simulations have also shown that the efficiency of outward transport of dust is weakly sensitive to the angular velocity Ω_{sp} of stellar spirals. For instance, a stellar spiral with $\Omega_{\mathrm{sp}} = 21$ km s^{-1} kpc^{-1} can transport roughly 1% less dust (see the dotted line in Fig. 8) than a spiral with $\Omega_{\mathrm{sp}} = 24$ km s^{-1} kpc^{-1}. We note that the corotation radius for $\Omega_{\mathrm{sp}} = 21$ km s^{-1} kpc^{-1} is at 8.8 kpc.

The solid line in Fig. 8b shows the gas mass inside corotation as a percentage of the total initial gas mass. [2] It is evident that the gas (contrary to the dust) does

[2] Due to the imposed outflow outer boundary condition, we cannot reliably calculate the gas mass outside corotation because its value can be affected by the

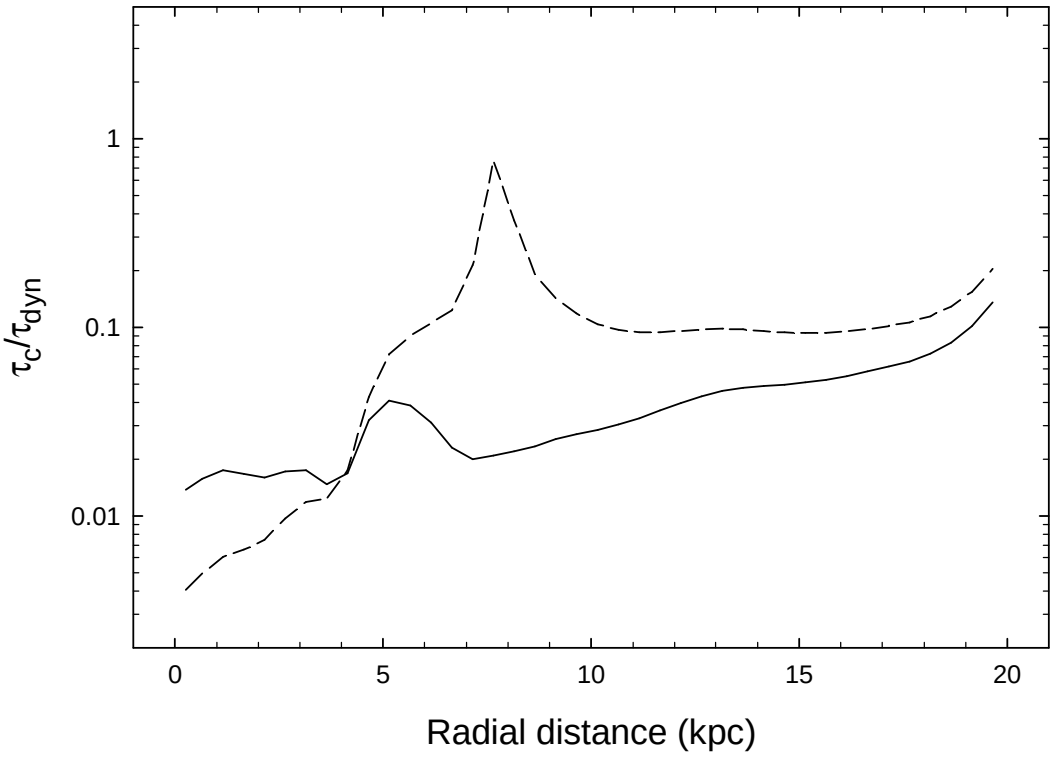

Fig. 9. The ratio of the frictional timescale $\tau_{\rm c}$ to the dynamical timescale $\tau_{\rm dyn}$ as a function of radius at $t = 1340$ Myr. The solid and dashed lines show $\tau_{\rm c}/\tau_{\rm dyn}$ for the dynamical timescale defined as $\tau_{\rm dyn} = \Omega_{\rm d}^{-1}$ and $\tau_{\rm dyn} = |\Omega_{\rm d}^{-1} - \Omega_{\rm sp}^{-1}|$, respectively. The detailed explanation is given in the text.

not exhibit a noticeable radial migration. A very weak inward radial transport ($\sim 1\%$ by mass) is seen for $\Omega_{\rm sp} = 24$ km s^{-1} kpc^{-1}, and it becomes negligible for $\Omega_{\rm sp} = 21$ km s^{-1} kpc^{-1}. We attribute this difference between the gas and dust radial transport rates to the restoring force of the pressure gradients which are always present in the warm ($T_{\rm g} \sim 10^4$ K) gas. The warm gas resists radial redistribution by creating additional pressure gradients which act to restore the initial centrifugally balanced configuration. The dust, however, is cold and it can easily flow in the radial direction provided that the coupling between dust and gas is not very strong.

To determine the main cause of the radial transport of dust, we compute the quantity $\tau_{\rm c}/\tau_{\rm dyn}$ (averaged over 0.5 kpc radial annuli). This quantity as a function of radius is shown by the solid line in Fig. 9 at the time when the gas spiral is fully developed. The collisional timescale $\tau_{\rm c}$ of energy and momentum exchange between the dust and gas particles is defined in Eq. (4). The local dynamical timescale is defined as $\tau_{\rm dyn} = \Omega_{\rm d}^{-1} = r/v_{{\rm d},\phi}$, where $v_{{\rm d},\phi}$ is the azimuthal component of dust velocity $\boldsymbol{v}_{\rm d}$. If $\tau_{\rm c} \ll \tau_{\rm dyn}$ the dust is expected to be strongly frictionally coupled to the gas and to essentially track the gas

gas that leaves the computational area. The dust, however, never reaches the outer boundary.

motion. Figure 9 shows that τ_c is a factor of $0.01-0.1$ smaller than τ_{dyn}, which implies a strong frictional coupling betwen dust and gas. However, judging from the bottom panels of Fig. 7, it would appear that the dust does not follow exactly the gas motion in the region near corotation. The reason is that the dust particles have natural resonant frequencies near corotation (remember that corotation determines the position of resonance in gas/dust orbits). If the gravitational field generated by spiral structure perturbs a dust particle's orbit at or near its resonant frequency, then the responce of the orbit will be large, even when the perturbing field is weak and/or the frictional coupling is strong. To investigate this effect, we re-define the local dynamical time as $\tau_{dyn} = |\Omega_d^{-1} - \Omega_{sp}^{-1}|$ and plot the corresponding quantity τ_c/τ_{dyn} in Fig. 9 by the dashed line. It is now evident that the frictional coupling between dust and gas is much weaker near corotation. This is consistent with the trajectories of dust particles found in Sect. 4 – only the dust particles that are born near corotation show substantial radial migration.

Another source of uncertainty in our simulations is the friction coefficient A, which we have adopted in the form of Eq. (4) to simplify the computations. As is pointed out in Sect. 2.1, the total stellar+gas surface density $\Sigma_s + \Sigma_g$ (instead of simply gas surface density, Σ_g) should appear in the definition of the gas vertical scale height

$$z_0 = \frac{c_s^2}{\pi G(\Sigma_s + \Sigma_g)}, \tag{14}$$

which may considerably increase the value of A. The uncertainity in the value of Σ_s (we do not explicitly follow the evolution of the stellar disk) works against this re-definition of z_0 in our simulations. In order to estimate the effect that the increased surface density of gravitating matter in Eq. (14) may have on the radial transport of dust particles, we notice that in the region of interest near corotation the ratio of stellar-to-gas surface densities is usually in the $1.5-15$ range. Therefore we performed a test run in which A was defined by Eq. (4), but was later multiplied by a factor of 10. The efficiency of outward radial transport of dust increased by less than 1%. In another test, A is decreased by a factor of 10, and the efficiency of outward radial transport of dust is dropped by approximately 1%. We conclude that an order of magnitude variation in A has a minor effect on the efficiency of radial transport of dust. This reinforces a previous conclusion: the resonant region near corotation, where $\Omega_d \approx \Omega_{sp}$, and the collisional drag force is dynamically less important than the spiral gravitational field, determines the radial migration of dust.

6 Dust destruction

In this section we study the effect of dust destruction by SNe on the efficiency of radial transport of dust in spiral galaxies. The dust grain destruction by SNe is the most important mechanism for cycling the dust back to the gas phase. The dust destruction rate can be determined as (Dwek, 1998)

$$D_{\rm d}(r,\phi,t) = m_{\rm dest}(r,\phi,t)\,\nu(r,\phi,t). \tag{15}$$

Here, $\nu(r,\phi,t)$ is the supernova rate per unit area and $m_{\rm dest}(r,\phi,t)$ is the mass of dust that is destroyed by a single SN expanding at location (r,ϕ) and time t. Only SN remnants with velocities exceeding 100 km s^{-1} can efficiently destroy dust grains. Therefore, the value of $m_{\rm dest}(r,\phi,t)$ is usually estimated from the relation $m_{\rm dest}/M_{\rm d} = \epsilon M_{\rm g}^{100}/M_{\rm g}$, where $M_{\rm g}^{100} = 3.8\times10^3\ M_\odot$ (Lisenfeld and Ferrara, 1998) is the mass of a remnant accelerated to velocities > 100 km s^{-1} by the blast. This relation simply states that the fraction of destroyed dust (by mass) within a computational cell is directly proportional to the fraction of accelerated remnant mass. The efficiency of dust destruction is $\epsilon \sim 0.1$ (McKee, 1989).

The SN rate per unit area is defined as

$$\nu(r,\phi,t) = \frac{\int_{9M_\odot}^{m_{\rm up}} \Sigma_{\rm SFR}(r,\phi,t-\tau(m))\,m^{-\alpha}\,dm}{\int_{m_{\rm low}}^{m_{\rm up}} m^{1-\alpha}dm}, \tag{16}$$

where $\Sigma_{\rm SFR}$ is the star formation rate per unit area, α is the slope of initial mass function (IMF), $\tau(m)$ is the lifetime of a star of mass m, $m_{\rm low}$ and $m_{\rm up}$ are the lower/upper cutoff masses, respectively. In practice, we approximate the integral in Eq. (16) by the sum with a mass discritization $dm = 1\ M_\odot$.

Observations of both normal and starburst disk galaxies suggest that on the scales of a few kiloparsecs star formation may be represented by a Schmidt law (Kennicutt, 1998)

$$\Sigma_{\rm SFR}\ \left(\frac{M_\odot}{\rm yr\ kpc^2}\right) = 2.5\times10^{-4}\ \Sigma_{\rm g}^{1.5}\ \left(\frac{M_\odot}{\rm pc^2}\right). \tag{17}$$

We modify the star formation law (17) by assuming that star formation is suppressed when $\Sigma_{\rm g} < min(\Sigma_{\rm crit}^{\rm Toomre}, \Sigma_{\rm crit}^{\rm shear})$.

Often, the instantaneous recycling approximation is used to solve Eq. (15), which neglects the time delay that enters Eq. (15) through the SN rate ν.

However, we follow a more accurate approach and form stellar clusters each Myr according to the star formation law (17). Stellar clusters are assigned positions and velocities drawn from the parent gas and are evolved as collisionless particles in the combined gravitational potential of the halo and stellar disk. The local self-gravity among stellar clusters is neglected. Since each stellar cluster carries information on the star formation rate at the time of its birth, the supernova rate $\nu(r,\phi,t)$ and the dust destruction rate $D_{\rm d}(r,\phi,t)$ in each computational cell (r,ϕ) at a time t can be easily obtained. This approach was successfully applied by Vorobyov (2003) to model the $H\alpha$ luminosity in ring galaxies. We use the Salpeter IMF with $\alpha = 2.35$ and lower/upper cutoff masses $m_{\rm low} = 0.5\ M_\odot$ and $m_{\rm up} = 40\ M_\odot$, respectively.

We modify the hydrodynamic equations (1)-(3) of our gas+dust system to take into account star formation and dust destruction. The continuity equations for the gas and dust become

$$\frac{\partial \Sigma_{\rm g}}{\partial t} + \boldsymbol{\nabla}\cdot(\Sigma_{\rm g}\,\boldsymbol{v}_{\rm g}) = S_{\rm g} - D_{\rm g}, \tag{18}$$

$$\frac{\partial \Sigma_{\rm d}}{\partial t} + \boldsymbol{\nabla}\cdot(\Sigma_{\rm d}\,\boldsymbol{v}_{\rm d}) = -D_{\rm d}. \tag{19}$$

The resulting momentum equations are

$$\frac{\partial}{\partial t}\Sigma_{\rm g}\boldsymbol{v}_{\rm g} + (\boldsymbol{v}_{\rm g}\cdot\boldsymbol{\nabla})\Sigma_{\rm g}\boldsymbol{v}_{\rm g} = -\Sigma_{\rm g}\boldsymbol{\nabla}\Phi_{\rm s1,s2,h} - \boldsymbol{\nabla}P_{\rm g} + \Sigma_{\rm d}\boldsymbol{f} + \boldsymbol{v}_{\rm g}(S_{\rm g} - D_{\rm g}), \tag{20}$$

$$\frac{\partial}{\partial t}\Sigma_{\rm d}\boldsymbol{v}_{\rm d} + (\boldsymbol{v}_{\rm d}\cdot\boldsymbol{\nabla})\Sigma_{\rm d}\boldsymbol{v}_{\rm d} = -\Sigma_{\rm d}\boldsymbol{\nabla}\Phi_{\rm s1,s2,h} - \Sigma_{\rm d}\boldsymbol{f} - \boldsymbol{v}_{\rm d}D_{\rm d}. \tag{21}$$

We have rewritten equations of motion in the form of momentum equations for $\Sigma\,\boldsymbol{v}$ which are appropriate for the system with sources and sinks. Star formation depletes the gas reservoir of our model galaxy and is taken into account by the sink term $D_{\rm g} = \Sigma_{\rm SFR}$ in Eqs. (18) and (20). The gas is returned to the system with supernova explosions and quiet mass loss of intermediate and low mass stars. Since we do not use a multiphase description of the interstellar medium, the ejected hot gas is directly transformed into a warm ($T \sim 10^4$ K) phase. The rate of gas ejection per unit area is determined by

$$S_{\rm g} = \frac{\int\limits_{m_{\rm low}}^{m_{\rm up}} g(m)\,\Sigma_{\rm SFR}(r,\phi,t-\tau(m))\,m^{-\alpha}\,dm}{\int\limits_{m_{\rm low}}^{m_{\rm up}} m^{1-\alpha}dm}, \tag{22}$$

where $g(m)$ denotes the gas mass ejected by a star of mass m (Köppen and Arimoto, 1991). We found it computationally prohibitive to compute accurately (i.e. by taking into account the time delay $\tau(m)$ in Eq. [22]) the gas ejection rate by stellar clusters on a time scale of interest (a few Gyr). Therefore, for the stellar clusters older than 100 Myr, the instantaneous recycling approximation is assumed by neglecting the time delay in Eq. (22). These stellar clusters instantaneously release all gas that can be produced by the $0.5 - 5\ M_{\odot}$ stars. Further dynamical evolution of such clusters is not computed.

We study the effect of dust destruction on the radial transport of dust using a prototype model in which the spiral density wave has a pitch angle $i = 25^{\circ}$ and angular velocity $\Omega = 24$ km s^{-1} kpc^{-1}. This model was studied in detail in Sect. 5 where we neglected the effect of dust destruction. It was shown there that about 10% of dust by mass injected instantaneously inside the corotation circle can be transported outside this region by the gravitational drag associated with spiral density waves. We reproduce this result in Fig. 10a by the dashed line, and the solid line gives the dust mass outside corotation as a percentage of the initial total dust mass when dust destruction is taken into account. As is seen, supernova explosions have a minor effect on the radial transport of dust, decreasing the relative amount of dust outside corotation by only 2% when compared to the model without dust destruction. It is worth noting that inside corotation the destruction of dust by supernova explosions is efficient. Indeed, the dashed-dotted and dotted lines in Fig. 10b show the dust mass inside corotation as a percentage of the initial total dust mass when dust destruction is taken and not taken into account, respectively. Approximately 15% of the instantaneously injected dust mass is left inside corotation after 2 Gyr. Given that another 10% has been transported outside corotation, SNe have destroyed about 75% of the injected dust mass during 2 Gyr. In Sect. 5 we argued that the ultimate fate of dust grains would depend on their place of birth. The simulations discussed in this section reinforce our earlier conclusion. In our model dust grains are formed inside the corotation circle at $r_{\rm cr} \approx 8$ kpc. The dust grains that are born in the inner 6.0 kpc circle (by implication they constitute the majority of the total dust mass) move on elliptic orbits periodically crossing the spiral arms and will be inevitably destroyed by supernova explosions after several revolution periods. However, the dust grains that are born in the 6 kpc $\lesssim r < 8$ kpc annulus and sufficiently away from spiral arms (by implication they constitute the minority of the total dust mass) manage to survive the destructive effect of supernova explosions during many revolution periods of our model galaxy. These dust grains may move on orbits similar to those shown in Fig. 5 by the solid and dotted lines, circulating between the spiral arms (but never crossing them) and periodically traveling in and out of the corotation circle. We conclude that a (small) portion of dust grains may survive the destructive effect of SNe during many (> 10) revolution periods of a spiral galaxy.

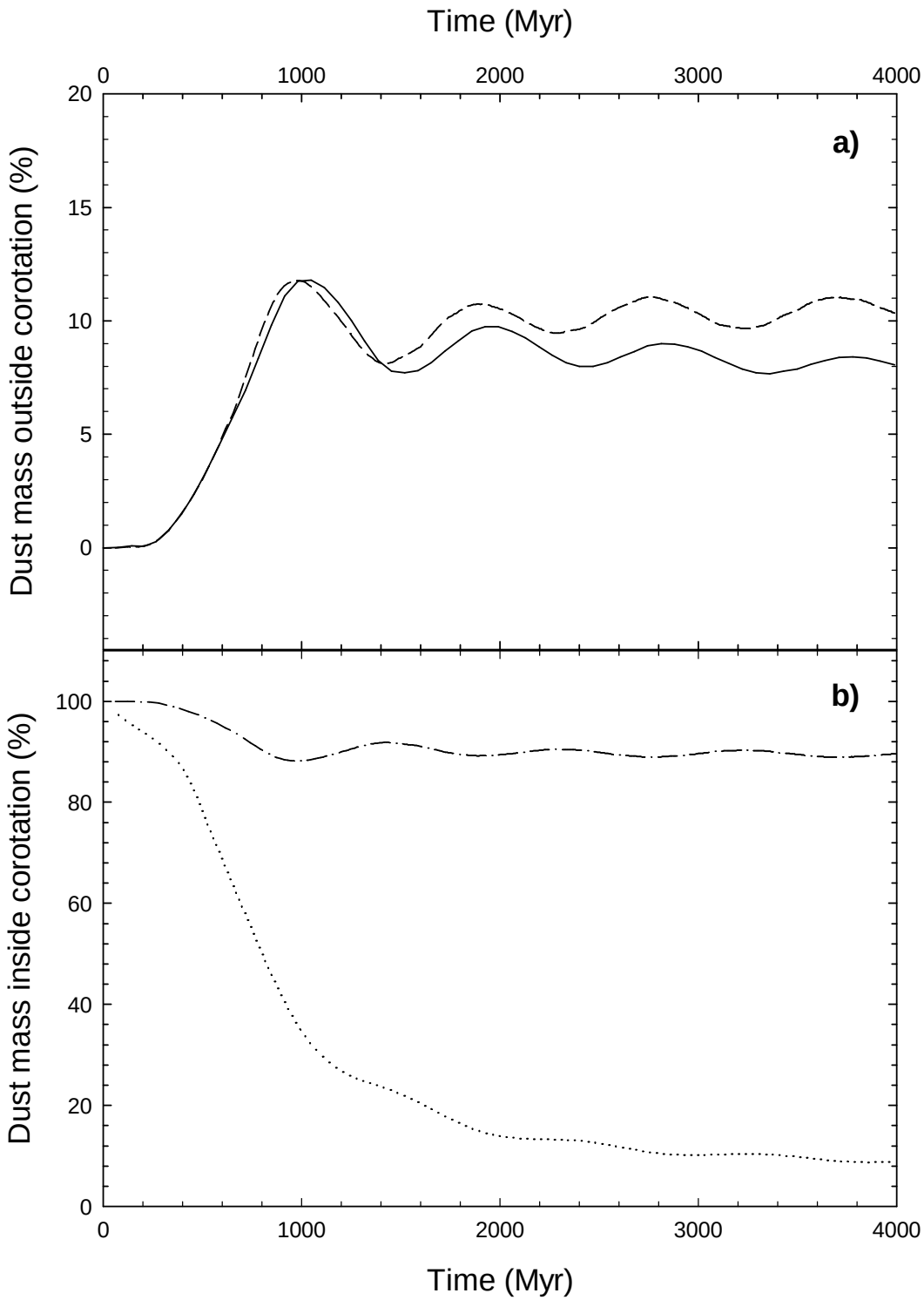

Fig. 10. **a)** Dust mass outside and **b)** inside corotation as a percentage of the total initial dust mass. The solid and dashed lines show the relative dust mass outside corotation in the models with and without dust destruction, respectively. The dotted and dotted-dashed lines give the relative dust mass inside corotation in the models with and without dust destruction, respectively.

7 Summary

In this paper we study the outward radial transport of interstellar dust grains which is connected with the perturbation of circular motions caused by spiral stellar density waves in disk galaxies. We consider a model spiral galaxy in which star formation (and, by implication, dust formation) is localized within the corotation circle. We find that the combined action of the gravity force of spiral stellar density waves and the drag force between the gas and dust components imparts to dust particles a radial velocity component, and thus can evacuate dust outward. We conclude that:

1. Dust grains that are formed inside corotation can be transported to a distance that exceeds the corotation radius by roughly 25%. In particular, if corotation is located at $r_{\rm cr} = 8.0$ kpc, dust grains formed inside the 6 kpc $\lesssim r <$ 8.0 kpc annulus can travel to distances as large as 10 kpc in roughly 1.0 Gyr. This is approximately an order of magnitude faster that can be provided by the interstellar turbulence.

2. A fraction of dust grains can be trapped into the interarm region, and thus can escape a hostile environment from supernova explosions acting mostly in the spiral arms. These grains form diffuse spiral arms which extend 4-5 kpc from the sites of active star formation. Dust particles that cross the spiral arms during their drift outward can survive if they do not meet strong shocks from SNe while passing through the arm.

3. In the model that considers instantaneous dust injection, about 10% of dust by mass is evacuated outside the corotation circle in roughly 1.0 Gyr. One can assume that continuous injection will result in the same percentage of evacuated dust. The efficiency of outward radial dust transport is weakly sensitive to the rotation speed of stellar spirals, but it may be considerably reduced for very tightly wound spirals with a pitch angle $i \lesssim 5^\circ$. Dust destruction by supernova explosions has only a minor effect on the efficiency of outward radial transport of dust by spiral density waves, which decreases the relative amount of transported dust mass by $\sim 2\%$. A (small) portion of dust grains may survive the destructive effect of SNe during many (> 10) revolution periods of a spiral galaxy.

4. Our modeling shows that the dust-to-gas ratio in the region near corotation (± 2 kpc) can vary substantially over the scales comparable to the thickness of spiral arms, ~ 1 kpc. Possible observations of such variations would be suggestive of the proposed mechanism of radial dust transport.

In our model we neglected the fact that charged dust grains are strongly coupled to the magnetic field – the gyration frequency for a typical grain with radius $a \sim 0.1\mu$m and grain charge $Z \sim 100$ is of $\omega_B \sim 10^{-10}$ Hz. We

expect that in more realistic models, where the magnetic field is permanently regenerated by a turbulent dynamo, dust particles will be involved in both the turbulent diffusive motions and regular flow, and the overall picture will remain qualitatively similar to that described above. We leave this issue for further study.

We should mention that the interaction of gas and solid particles through the drag force and the associated radial flow of solid particles have been already extensively studied in the context of migration of planetisimals in protoplanetary disks. For example, Weidenschilling (1977) has noticed that in protoplanetary disks the planetesimals should migrate in the direction of increasing pressure (i.e. inward, for an axisymmetric disk with a declining radial density profile). This is due to the fact that the gas in protoplanetary disks generally orbits the central protostar at the sub-Keplerian velocity due to a substantial contribution of pressure gradients in the gas rotation curve. The cold planetesimals (which by implication have no pressure) are then forced to flow inward if the frictional orbital coupling between the gas and planetesimals is not too strong. This mechanism however may not work on galactic scales because the contribution of the pressure gradients to the gas rotation velocity may be negligible (see Sect. 2.2). In fact, the pressure gradients may even assist the gravity in some disk galaxies with a ring-like radial distribution of gas. Another interesting aspect of gas-planetesimal interaction in self-gravitating, protoplanetary disks was investigated by Rice et al. (2004). They considered disks with a flocculent spiral structure and demonstrated that the drag force rather than gravitational field of spiral arms plays a dominant role in the dynamics of planetesimals of intermediate size, forcing them to concentrate in the gas spiral arms. The non-axisymmetric gravitational field of grand-design spirals (considered in the present paper) is by implication much stronger than that of flocculent spirals. As a consequence, the trajectories of dust particles can be considerably influenced by the spiral gravitatioanl field (Fig. 5). We believe that the resonant action of spiral gravitational field on dust particles (rather than the drag force between the gas and dust) is the main driving force for the radial outward transport of dust in grand-design spiral galaxies. This conjecture is justified by the fact that the radial flow of dust takes place near the corotation resonance where a weaker frictional coupling between the dust and gas occurs (see Fig. 9).

Acknowledgements

We are grateful to Dr. Carol Jones for carefully reading the manuscript and correcting the English language usage. We are thankful to the anonymous referee for an insightful report that helped improve the final presentation. EIV gratefully acknowledges present support from a CITA National Fellowship.

Part of this work (YS) was supported by *Deutsche Forschungsgemeinschaft, DFG* (project SFB TP B3). The simulations were partly performed on the Shared Hierarchical Academic Research Computing Network (SHARCNET) cluster.

References

Bianchi, S., Alton, P. B., Davies, J. I., 2000, in: ISO Beyond Point Sources, R. J. Laureijs, K. Leech, M. F. Kessler, eds., p. 149

Binney, J., Tremaine, S. 1987, Galactic Dynamics (Princeton: Princeton Univ. Press)

Cho, J., Lazarian, A., Honein, A., Knaepen, B., Kassinos, S., Moin, P., 2003. ApJ, 589, L77

Dettmar, R.-J., Shaginyan, A. S., Shchekinov, Yu. A., 2005. A&A, submitted

Draine, B. T., Salpeter, E. E., 1979. ApJ 213, 77

Dwek, E. 1998., ApJ 501, 643

Ferrara, A., Ferrini, F., Barsella, B., Franco, J., 1991. ApJ 381, 137

Gómez, G. C., Cox, D. P., 2002. ApJ 580, 235

Howk, J.C., Savage, B.D., 1997. AJ 114, 2463

Howk, J.C., Savage, B.D., 1999. AJ 117, 2077

Kennicutt, R. C., 1981. AJ 86, 1847

Kennicutt, R. C., 1989. ApJ 344, 658

Kennicutt, R. C. 1998, ApJ, 498, 541

Köppen, J., & Arimoto, N. 1991, A&AS, 87, 109

Lin, C. C., Yuan, C., Shu, F. H., 1969. ApJ 155, 721

Lisenfeld, U., Ferrara, A., 1998, ApJ 496, 145

Mac Low, M.-M., Ferrara, A., 1999. ApJ 513, 142

Martin, C., Kennicutt, R. C., 2001. ApJ 555, 301

McKee, C. F. 1989, in IAU Symp. 135, Interstellar Dust, ed. L. J. Allamandola, A. G. G. M. Tielens (Dordrecht:Kluwer), 431

Neininger, N., Guélin, M., García-Burillo, S., Zylka, R., Wielebinski, R., 1996. A&A 310, 725

Noh, H., Vishniac, E. T., Cochran, W. D., 1991. ApJ 383, 372

Norman, C.A. Ikeuchi, S., 1989. ApJ 345, 372

Rice, W. K. M., Lodato, G., Pringle, J. E., Armitage, P. J., Bonnell, I. A., 2004, MNRAS, 355, 543

Rossa, J., Dettmar, R.-J., Walterbos, R. A. M., Norman, C. A., 2004. AJ 128, 674

Shustov, B. M., Vibe D. Z., 1995. Astron. Rept 39, 578

Silich, S., Tenorio-Tagle, G., 2001. ApJ 552, 91

Spitzer, L. 1978, Physical Processes in the Interstellar Medium, (New York: Wiley)

Stone, J., M., Norman, M. L., 1992. ApJS 80, 753

Thompson, T. W. J., Howk, J. C., Savage, B. D., 2004. AJ, 128 662

Toomre, A., 1963. ApJ 138, 385

Trewhella, M., Davies, J. I., Alton, P. B., Bianchi, S., 2000. ApJ 543, 153

Vorobyov, E. I., 2003. A&A, 407, 913

Weidenschilling, S., 1977, MNRAS, 180, 57

Weingartner, J. C., Draine, B. T., 2001. ApJ 553, 581

Xilouris, E. M., Byum, Y. I., Kylafis, W. D., Paleologou, E. V., Papamastorakis, J., 1999. A&A 344, 868

Yan, H., Lazarian, A., Draine, B. T., 2004. ApJ 616, 895